# A Survey of Various Propagation Models for Mobile Communication

Tapan K. Sarkar[1], Zhong Ji[1], Kyungjung Kim[1], Abdellatif Medouri[2], and Magdalena Salazar-Palma[3]

[1]Department of Electrical Engineering and Computer Science
Syracuse University
121 Link Hall, Syracuse, New York 13244-1240, USA
Tel: 1 (315) 443-3775; Fax: 1 (315) 443-4441; E-mail: tksarkar@syr.edu

[2]Ecole Nationale des Sciences Appliquées
Abdelmalek Essadi University
Tangier, Morocco
E-mail: amedouri@ieee.org

[3]Grupo de Microondas y Radar, Dpto. Senales, Sistemas y Radiocommunicacion, ETSI Telecommunication
Universidad Politecnica de Madrid
Ciudad Universitaria, 28040 Madrid, Spain
E-mail: Salazar@gmr.ssr.upm.es

## Abstract

In order to estimate the signal parameters accurately for mobile systems, it is necessary to estimate a system's propagation characteristics through a medium. Propagation analysis provides a good initial estimate of the signal characteristics. The ability to accurately predict radio-propagation behavior for wireless personal communication systems, such as cellular mobile radio, is becoming crucial to system design. Since site measurements are costly, propagation models have been developed as a suitable, low-cost, and convenient alternative. Channel modeling is required to predict path loss and to characterize the impulse response of the propagating channel. The path loss is associated with the design of base stations, as this tells us how much a transmitter needs to radiate to service a given region. Channel characterization, on the other hand, deals with the fidelity of the received signals, and has to do with the nature of the waveform received at a receiver. The objective here is to design a suitable receiver that will receive the transmitted signal, distorted due to the multipath and dispersion effects of the channel, and that will decode the transmitted signal. An understanding of the various propagation models can actually address both problems. This paper begins with a review of the information available on the various propagation models for both indoor and outdoor environments. The existing models can be classified into two major classes: statistical models and site-specific models. The main characteristics of the radio channel – such as path loss, fading, and time-delay spread – are discussed. Currently, a third alternative, which includes many new numerical methods, is being introduced to propagation prediction. The advantages and disadvantages of some of these methods are summarized. In addition, an impulse-response characterization for the propagation path is also presented, including models for small-scale fading. Finally, it is shown that when two-way communication ports can be defined for a mobile system, it is possible to use reciprocity to focus the energy along the direction of an intended user without any explicit knowledge of the electromagnetic environment in which the system is operating, or knowledge of the spatial locations of the transmitter and the receiver.

Keywords: Land mobile radio cellular systems; land mobile radio propagation factors; communication channels; multipath channels; fading channels; transient response; reciprocity

## 1. Introduction

The commercial success of cellular communications, since its initial implementation in the early 1980s, has led to an intense interest among wireless engineers in understanding and predicting radio-propagation characteristics in various urban and suburban areas, and even within buildings. As the explosive growth of mobile communications continues, it is very valuable to have the capability of determining optimum base-station locations, obtaining suitable data rates, and estimating their coverage, without conducting a series of propagation measurements, which are very expensive and time consuming. It is therefore important to develop effective propagation models for mobile communications, in order to provide design guidelines for mobile systems.

# 2. Definitions and Terminology used for Characterizing Various Parameters of a Propagation Channel

In order to understand the nature of the models that are going to be presented, several definitions and the terminology for both narrowband and wideband wave propagation over a radio channel are first described, in order to familiarize the reader with the terminology and parameters of the problem.

## 2.1 Path Loss

Path loss (PL) is a measure of the average RF attenuation suffered by a transmitted signal when it arrives at the receiver, after traversing a path of several wavelengths. It is defined by [1]

$$PL(dB) = 10 \log \frac{P_t}{P_r}, \qquad (1)$$

where $P_t$ and $P_r$ are the transmitted and received power, respectively. In free space, the power reaching the receiving antenna – which is separated from the transmitting antenna by a distance $d$ – is given by the Friis free-space equation:

$$P_r = (d) \frac{P_t G_t G_r \lambda^2}{(4\pi)^2 d^2 L}, \qquad (2)$$

where $G_t$ and $G_r$ are the gain of the transmitting and the receiving antenna, respectively. $L$ is the system loss factor, not related to propagation. $\lambda$ is the wavelength in meters. It is clear that Equation (2) does not hold for $d = 0$. Hence, many propagation models use a different representation for a close-in distance, $d_0$, known as the received-power reference point. This is typically chosen to be 1 m. In realistic mobile radio channels, free space is not the appropriate medium. A general PL model uses a parameter, $\gamma$, to denote the power-law relationship between the separation distance and the received power. So, path loss (in decibels) can be expressed as [2]

$$PL(d) = PL(d_0) + 10\gamma \log(d/d_0) + X_\sigma, \qquad (3)$$

where $\gamma = 2$ characterizes free space. However, $\gamma$ is generally higher for wireless channels. $X_\sigma$ denotes a zero-mean Gaussian random variable of standard deviation $\sigma$, which reflects the variation, on average, of the received power that naturally occurs when a PL model of this type is used. Path loss is the main ingredient of a propagation model. It is related to the area of coverage of mobile systems.

## 2.2 Power-Delay Profile

Random and complicated radio-propagation channels can be characterized using the impulse-response approach. For each point in the three-dimensional environment, the channel is a linear filter with impulse response $h(t)$. The impulse response provides a wideband characterization of the propagating channel, and contains all of the information necessary to simulate or analyze any type of radio transmission through that channel.

Multipath propagation causes severe dispersion of the transmitted signal. The expected degree of dispersion is determined through the measurement of the power-delay profile of the channel. The power-delay profile provides an indication of the dispersion or distribution of transmitted power over various paths in a multipath model for propagation. The power-delay profile of the channel is calculated by taking the spatial average of $|h(t)|^2$ over a local area. By making several local-area measurements of $|h(t)|^2$ for different locations, it is possible to build an ensemble of power-delay profiles, each one representing a possible small-scale multipath channel state [3, 10]. A typical plot of the power-delay profile is shown in Figure 1.

Many multipath-channel parameters are derived from the power-delay profile. Power-delay profiles are measured using wideband channel-sounding techniques, and are presented in the form of plots of the received power as a function of an additional or excess delay with respect to a fixed time-delay reference. There is a delay between the time of transmission of the signal and when it is received, due to the finite velocity of propagation of the electromagnetic signal. However, additional delay may be introduced by the propagation medium, as well. A mobile channel exhibits a continuous multipath structure; hence, the power-delay profile can be thought of as a density function, of the form

$$P(\tau) = \frac{|h(t)|^2}{\int_{-\infty}^{\infty} |h(t)|^2 \, dt}. \qquad (4)$$

## 2.3 Time-Delay Spread

Time dispersion varies widely in a mobile radio channel, due to the fact that reflections and scattering occur at seemingly random locations, and the resulting multipath channel response appears random, as well. Because time dispersion is dependent on the geometrical position relationships among the transmitter, the receiver, and the surrounding physical environment, some parameters that can grossly quantify the multipath channel are used. They are described in the following subparagraphs.
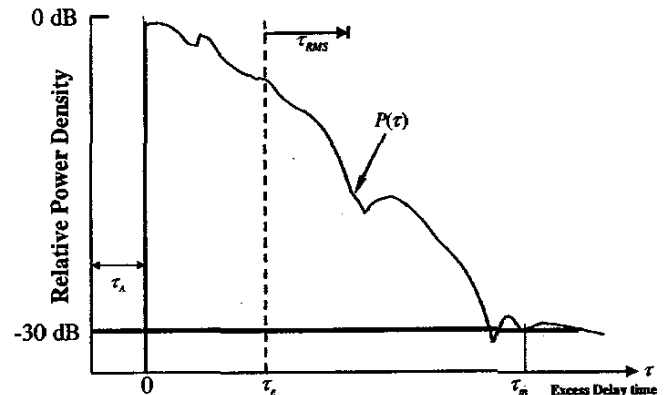


Figure 1. An illustration of a typical power-delay profile and the definition of the delay parameters.

### 2.3.1 First-Arrival Delay ($\tau_A$)

This is a time delay corresponding to the arrival of the first transmitted signal at the receiver. It is usually measured at the receiver. This delay is set by the minimum possible propagation-path delay from the transmitter to the receiver. It serves as a reference, and all delay measurements are made relative to it. How the origin is defined is seen in Figure 1. Any measured delay longer than this reference delay is called an excess delay.

### 2.3.2 Mean Excess Delay ($\tau_e$)

This is the first moment of the power-delay profile (as shown in Figure 1) with respect to the first delay. It is expressed as

$$\tau_e = \int (\tau - \tau_A) P(\tau) d\tau . \qquad (5)$$

### 2.3.3 RMS Delay ($\tau_{RMS}$)

This is the square root of the second central moment of a power-delay profile, as seen in Figure 1. It is the standard deviation about the mean excess delay, and is expressed as

$$\tau_{RMS} = \left[ \int (\tau - \tau_e - \tau_A)^2 P(\tau) d\tau \right]^{1/2} . \qquad (6)$$

The RMS delay is a good measure of the multipath spread. It gives an indication of the nature of the inter-symbol interference (ISI). Strong echoes (relative to the shortest path) with long delays contribute significantly to $\tau_{RMS}$. The effects of dispersion on the performance of a digital receiver can be reliably related only to it, independently of the shape of the power-delay profile, so long as it is small compared to the symbol period ($T$) of the digital modulation. It is also used to give an estimate of the maximum data rate for transmission.

### 2.3.4 Maximum Excess Delay ($\tau_m$)

This is measured with respect to a specific power level, which is characterized as the threshold of the signal. When the signal level is lower than the threshold, it is processed as noise. For example, the maximum excess delay spread can be specified as the excess delay ($\tau_m$) for which $P(\tau)$ falls below −30 dB with respect to its peak value, as shown in Figure 1.

### 2.4 Coherence Bandwidth

While the delay spread is a natural phenomenon caused by the reflection and scattering of the transmitted signal in a radio channel, the coherence bandwidth, $B_C$, is defined in terms of the RMS delay spread. It is a statistical measure of the range of frequencies over which the channel can be considered "flat." It is defined as the bandwidth over which the variation of the signal is about 10%, and is approximated by [4, 10]

$$B_C \approx \frac{1}{50\tau_{RMS}}. \qquad (7)$$

It is important to note that an exact relationship between the coherence bandwidth and the RMS delay spread does not exist. The real coherence bandwidth depends on the actual impulse response of the channel.

### 2.5 Types of Fading

The type of fading experienced by a signal propagating through a mobile radio channel depends on the nature of the transmitted signal, as well as on the characteristics of the channel. Different transmitted signals will undergo different types of fading, according to the relationship among the signal parameters, such as the path loss, the bandwidth (BW), the symbol period, etc., and the channel parameters (such as the RMS delay spread and the Doppler spread). Figure 2 describes the different types of fading and the different relationships that exist among them [5].

The phenomenon of large-scale fading is affected primarily by the presence of hills, forests, and buildings between the transmitter and the receiver. The statistics of large-scale fading provide a way of computing an estimate of the path loss as a function of distance and other factors.

A channel is said to exhibit frequency-selective fading when the delay spread is greater than the symbol period. This condition occurs whenever the received multipath components of a symbol extend beyond the time duration of the symbols. Such multipath dispersion of the signal yields a kind of inter-symbol interference (ISI) called channel-induced ISI. When the delay spread is less than the symbol period, a channel is said to exhibit flat fading, and there is no channel-induced ISI distortion. But there can still be performance degradation, due to the irresolvable phasor components that add up destructively to yield a substantial reduction in signal-to-noise ratio (SNR) at the receiver.

Fast fading and slow fading are classified on the basis of how rapidly the transmitted baseband signal changes, compared to the rate of the electrical-parameter changes of the channel. If the channel impulse response changes at a rate much faster than the transmitted signal, the channel may be assumed to be a fast-fading channel. Otherwise, it is assumed to be a slow-fading channel. It is important to note that the velocity of the mobile unit or the velocity of objects using the channel through a baseband signal determines whether a signal undergoes fast fading or slow fading.

### 2.6 Adaptive Antennas

An application of antenna arrays has been suggested in recent years for mobile communications systems, to overcome the problems of single-antenna systems. The use of adaptive antenna arrays helps improve the system's performance by increasing channel capacity and spectrum efficiency, extending range coverage, tailoring beam shape, steering multiple beams to track many mobiles, and electronically compensating for the aperture distortion. It also reduces multipath fading, co-channel interference, system complexity and cost, bit-error rate (BER), and outage probability [6].

A phased-array antenna uses an array of simple antennas, and combines the signal induced on the elements to form the output.
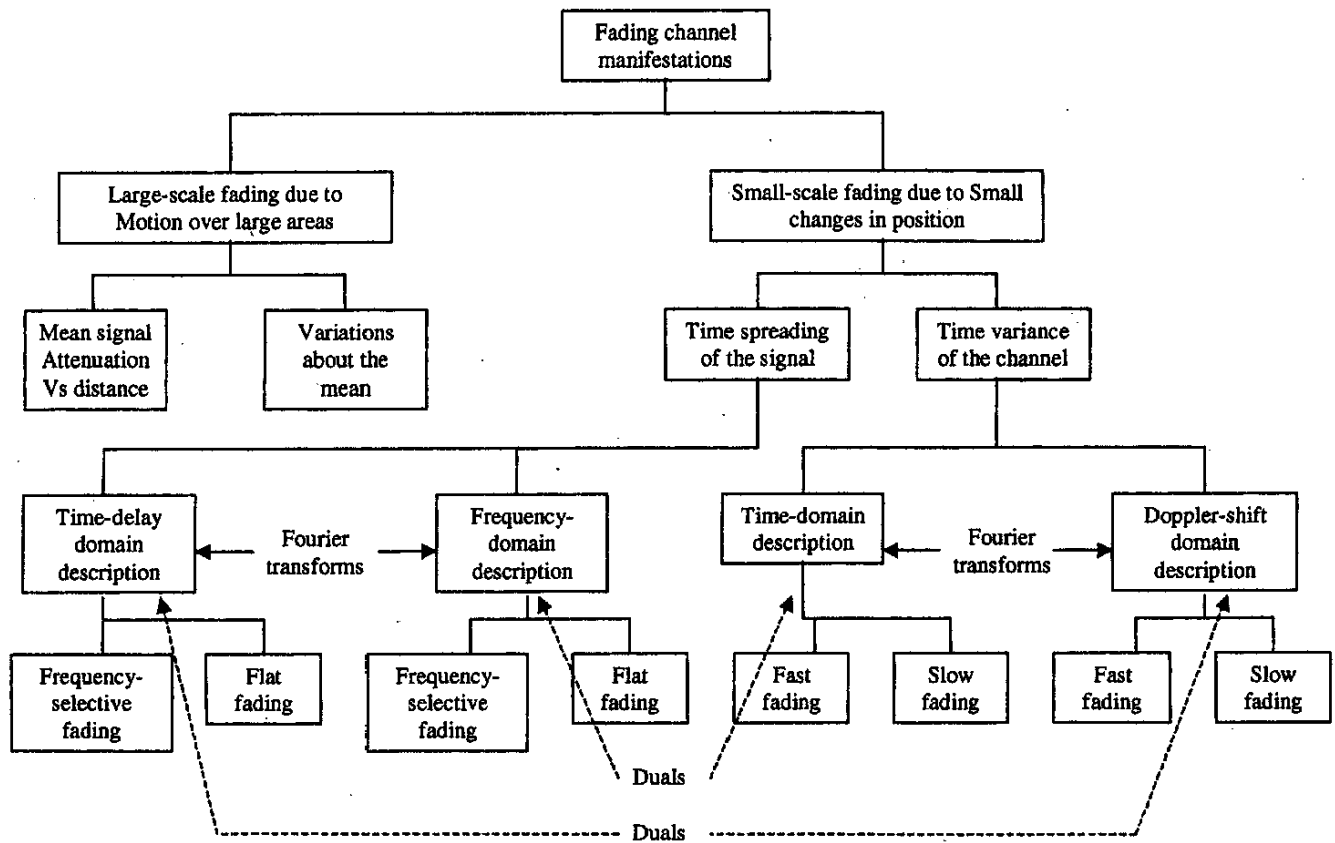
```
                          Fading channel
                          manifestations

        Large-scale fading due to          Small-scale fading due to Small
        Motion over large areas                 changes in position

   Mean signal        Variations        Time spreading      Time variance
   Attenuation        about the         of the signal       of the channel
   Vs distance          mean

 Time-delay      Fourier     Frequency-      Time-domain     Fourier    Doppler-shift
 domain          transforms  domain          description     transforms domain
 description                 description                                description

 Frequency-   Flat      Frequency-   Flat      Fast    Slow      Fast    Slow
 selective    fading    selective    fading    fading  fading    fading  fading
 fading                 fading

                                              Duals

                      ------------------  Duals  ------------------
```

**Figure 2. Different types of fading.**

The term "adaptive antenna" is used for a phased array when the gains and the phases of the signals induced in the various elements are weighted before combining to adjust the gain of the array in a dynamic fashion along a particular look direction, while simultaneously placing nulls along undesired directions.

The propagation models used for an adaptive antenna are different from those for a single antenna. Details of a phased-array antenna can be obtained in [6, 7].

# 3. Multipath Propagation

In a typical mobile-radio application, the base station is fixed in position, while the mobile unit is moving. This is usually subject to a condition such that the propagation between them is largely through scattering, either by reflection or diffraction from buildings and terrain or objects within buildings, because of obstruction of the line-of-sight (LOS) path. Radio waves therefore arrive at the mobile receiver from different directions with different amplitudes, phases, and time delays, resulting in a phenomenon known as multipath propagation. The radio channel is then obtained as the sum of the contributions from all of the paths. If the input signal is a unit impulse, $\delta(t)$, the output will be the channel impulse response, which can be written as [9]

$$h(t) = \sum_{n=1}^{N} A_n \delta(t - \tau_n) \exp(-j\varphi_n).$$  (8)

The channel impulse response can thus be characterized by $N$ time-delayed impulses, each represented by an attenuated and phase-shifted version of the original transmitted impulse. Here, $A_n$, $\tau_n$, and $\varphi_n$ are the attenuation, delay in time of arrival, and phase, corresponding to path $n$, respectively.

Although multipath interference seriously degrades the performance of communication systems, little can be done to eliminate it. However, if we characterize the multipath medium well, and have sound knowledge of the propagation mechanisms and their influence on the system, the best design for the system can be selected to achieve good propagation performance and, hence, to achieve a better quality of service.

## 3.1 Three Basic Propagation Mechanisms

Reflection, diffraction, and scattering are the three basic propagation mechanisms [10] that impact propagation in mobile communication systems. They are briefly explained below.

### 3.1.1 Reflection

Reflection occurs when a propagating electromagnetic wave impinges upon an object that has very large dimensions compared to the wavelength of the propagating wave. Reflection occurs from the surface of the ground, from walls, and from furniture. When

reflection occurs, the wave may also be partially refracted. The coefficients of reflection and refraction are functions of the material properties of the medium, and generally depend on the wave polarization, the angle of incidence, and the frequency of the propagating wave.

## 3.1.2 Diffraction

Diffraction occurs when the radio path between the transmitter and receiver is obstructed by a surface that has sharp edges. The waves produced by the obstructing surface are present throughout space and even behind the obstacle, giving rise to the bending of waves around the obstacle, even when a line of sight (LOS) path does not exist between the transmitter and receiver. At high frequencies, diffraction – like reflection – depends on the geometry of the object, as well as on the amplitude, phase, and polarization of the incident wave at the point of diffraction.

## 3.1.3 Scattering

Scattering occurs when the medium through which the wave propagates consists of objects with dimensions that are small compared to the wavelength, and where the number of obstacles per unit volume is large. Scattered waves are produced by rough surfaces, small objects, or by other irregularities in the channel. In practice, foliage, street signs, lampposts, and stairs within buildings can induce scattering in mobile-communication systems. A sound knowledge of the physical details of the objects can be used to accurately predict the scattered signal strength.

In most cases, the scattering can be neglected [11], and the complex field received from the various incident paths is given by [12]

$$\vec{E}_{receive} = \sum_i \vec{E}_i \, , \tag{9}$$

where

$$E_i = E_0 \wp_{ti} \wp_{ri} L_i(d) \prod_j \Gamma(\phi_{ji}) \prod_p T(\phi_{pi}) e^{-jkd} , \tag{10}$$

and

$E_0$ is the amplitude of the reference incident field (V/m); $\wp_{ti}$ and $\wp_{ri}$ are the transmitting- and receiving-antenna field radiation patterns along the direction of interest for the $i$th multipath component; $L_i(d)$ is the path-loss characterization for the $i$th multipath component; $\Gamma(\phi_{ji})$ is the reflection coefficient for the $j$th reflection of the $i$th multipath component; $T(\phi_{pi})$ is the transmission coefficient for the $p$th transmission of the $i$th multipath component; $e^{-jkd}$ is the propagation phase factor due to the path length $d$ ($k = 2\pi/\lambda$, with $\lambda$ representing the wavelength); $d$ is the path length (m); and $E_i$ is the field strength of the $i$th multipath component.

For diffraction, the product of the complex reflection and transmission coefficients is replaced by the complex diffraction coefficient.

## 3.2 Propagation in Outdoor and Indoor Environments

With the growth in the capacity of mobile communications, the size of a cell is becoming smaller and smaller: from macrocell to microcell, and then to picocell. The service environments include both outdoor and indoor areas.

When propagation is considered in an outdoor environment, one is primarily interested in three types of areas: urban, suburban, and rural areas. The terrain profile of a particular area also needs to be taken into account. The terrain profile may vary from a simple, curved Earth to a highly mountainous region. The presence of trees, buildings, moving cars, and other obstacles must also be considered. The direct path, reflections from the ground and buildings, and diffraction from the corners and roofs of buildings are the main contributions to the total field generated at a receiver, due to radio-wave propagation.

With the advent of personal communication systems (PCS), there is also a great deal of interest in characterizing radio propagation inside buildings. The indoor radio channel differs from the traditional outdoor mobile radio channel in two aspects: the distance covered is much smaller, and the variability of the environment is much greater for a much smaller range of transmitter and receiver separation distances [10]. Propagation into and inside buildings has, to some extent, a more complex multipath structure than an outdoor propagation environment. This is mainly because of the nature of the structures used for the buildings, the layout of rooms and, most importantly, the type of construction materials used. Table 1 represents the categories of buildings where propagation measurements have been made [13].

## 3.3 Summary of Propagation Models

In mobile communications, signals from the mobile unit arrive at a base station via multiple paths, each with its own angle of arrival (AOA), path delay, and attenuation. When the communication system uses an adaptive-processing methodology, it is also important to estimate the joint angle and delay for various signals.

There are two main models for characterizing path loss: empirical (or statistical) models, and site-specific (or deterministic) models. The former are based on the statistical characterization of the received signal. They are easier to implement, require less computational effort, and are less sensitive to the environment's

**Table 1. Classification of buildings.**

| Proposed Categories | |
| --- | --- |
| Category Number | Description |
| 1 | Residential houses in suburban areas |
| 2 | Residential houses in urban areas |
| 3 | Office buildings in suburban areas |
| 4 | Office buildings in urban areas |
| 5 | Factory buildings with heavy machinery |
| 6 | Other factory buildings, sports halls, exhibition centers |
| 7 | Open environment, e.g. railway stations, airports, etc. |
| 8 | Underground, e.g. subways, underground streets, etc. |

geometry. The latter have a certain physical basis, and require a vast amount of data regarding geometry, terrain profile, locations of building and of furniture in buildings, and so on. These deterministic models require more computations, and are more accurate.

Most models of fading apply stochastic processes to describe the distribution of the received signal. It is useful to use these models to simulate propagation channels and to estimate the performance of the system in a homogeneous environment. Models of time-delay spread, both for outdoor and indoor environments, are generally derived from a lot of measurements. Some of the propagation models have been discussed in [142], and here we have included additional, new models.

There is another parameter that is sometimes seen in the various models: this is the effect of the Doppler frequency on the channel characterization. The thinking is that since the mobile wireless receiver is moving, the Doppler shift is relevant to the model. If a mobile unit is operating at, say, 900 MHz, and is traveling at 150 km/hr, then we know that in this case the Doppler shift will be given by

$$f_{doppler} = \frac{2 \times 150000 \times 900 \times 10^6}{3600 \times 3 \times 10^8} = 250 \text{ Hz} . \quad (11)$$

It would be useful to study why such a small value of the Doppler shift will have an impact on the processing of a modulated 900 MHz signal.

# 4. Models for Path Loss

## 4.1 Empirical or Statistical Models for Path Loss

### 4.1.1 Outdoor Case

There are a number of empirical or statistical models suitable for both macrocell and microcell scenarios for the outdoor environment. Some of these are described below.

#### 4.1.1.1 Okumura et al. Model

This is one of the most widely used models for propagation in urban areas [14]. The model can be expressed as

$$L_{50}(\text{dB}) = L_F + A_{mu}(f,d) - G(h_{te}) - G(h_{re}) - G_{AREA}, \quad (12)$$

where $L_{50}$ is the median value of the propagation path loss, $L_F$ is the free-space propagation loss, $A_{mu}$ is the median attenuation in the medium relative to free space at frequency $f$, and $d$ corresponds to the distance between the base and the mobile unit. $G(h_{te})$ and $G(h_{re})$ are the gain factors for the base-station antenna and the mobile antenna, respectively. $h_{te}$ and $h_{re}$ are the effective heights of the base-station and the mobile antennas (in meters), respectively. $G_{AREA}$ is the gain generated by the environment in which the system is operating. Both $A_{mu}(f,d)$ and $G_{AREA}$ can be found from empirical curves. Okumura et al.'s model is considered to be

among the simplest and best in terms of accuracy in predicting path loss for early cellular systems. It is very practical, and has become a standard for system planning in Japan. The major disadvantage of this model is its slow response to rapid changes in terrain profile.

### 4.1.1.2 Hata Model

The Hata model is an empirical formulation [15] of the graphical path-loss data provided by Okumura's model. The formula for the median path loss in urban areas is given by

$$L_{50}(\text{urban})(\text{dB}) = 69.55 + 26.16 \log f_c - 13.82 \log h_{te}$$
$$-a(h_{re}) + (44.9 - 6.55 \log h_{te}) \log d, \quad (13)$$

where $f_c$ is the frequency (in MHz), which varies from 150 MHz to 1500 MHz. $h_{te}$ and $h_{re}$ are the effective heights of the base-station and the mobile antennas (in meters), respectively. $d$ is the distance from the base station to the mobile antenna, $a(h_{re})$ is the correction factor for the effective antenna height of the mobile unit, which is a function of the size of the area of coverage. For small- to medium-sized cities, the mobile-antenna correction factor is given by

$$a(h_{re}) = (1.1 \log f_c - 0.7) h_{re} - (1.56 \log f_c - 0.8) \text{dB} . \quad (14)$$

For a large city, it is given by

$$a(h_{re}) = 8.29(\log 1.54 h_{re})^2 - 1.1 \text{dB} \text{ for } f_c \le 300 \text{ MHz} \quad (15.a)$$

$$a(h_{re}) = 3.2(\log 11.75 h_{re})^2 - 4.97 \text{dB} \text{ for } f_c \ge 300 \text{ MHz} \quad (15.b)$$

To obtain the path loss in a suburban area, the standard Hata formula is modified as follows:

$$L_{50}(\text{dB}) = L_{50}(\text{urban}) - 2\left[\log(f_c/28)\right]^2 - 5.4 . \quad (16)$$

The path loss in open rural areas is expressed through

$$L_{50}(\text{dB}) = L_{50}(\text{urban}) - 4.78(\log f_c)^2 - 18.33 \log f_c - 40.98 . \quad (17)$$

This model is quite suitable for large-cell mobile systems, but not for personal communications systems that cover a circular area of approximately 1 km in radius.

### 4.1.1.3 COST-231-Walfisch-Ikegami Model

This model utilizes the theoretical Walfisch-Bertoni model [16], and is composed of three terms [17]:

$$L_b = \begin{cases} L_0 + L_{rts} + L_{msd} & \text{for } L_{rts} + L_{msd} > 0 \\ L_0 & \text{for } L_{rts} + L_{msd} \le 0 \end{cases}, \quad (18)$$

where $L_0$ represents the free-space loss. $L_{rts}$ is the "roof-top-to-street diffraction and scattering loss." $L_{msd}$ is the "multi-screen diffraction loss." The free-space loss is given by

$$L_0 = 32.4 + 20\log d + 20\log f \, , \tag{19}$$

where $d$ is the radio-path length (in km), $f$ is the radio frequency (in MHz), and

$$L_{rts} = -16.9 - 10\log w + 10\log f + 20\log \Delta h_{Mobile} + L_{ori} \, . \tag{20}$$

Here, $w$ is the street width (in m), and

$$\Delta h_{Mobile} = h_{Roof} - h_{Mobile} \tag{21}$$

is the difference between the height of the building on which the base-station antenna is located, $h_{Roof}$, and the height of the mobile antenna, $h_{Mobile}$. $L_{ori}$ is given by

$$L_{ori} = \begin{cases} -10 + 0.354\phi & 0° \le \phi < 35° \\ 2.5 + 0.075(\phi - 35) & \text{for} \quad 35° \le \phi < 55°, \\ 4.0 - 0.114(\phi - 55) & 55° \le \phi \le 90° \end{cases} \tag{22}$$

where $\phi$ is the angle of incidence relative to the direction of the street. $L_{msd}$ is given by

$$L_{msd} = L_{bsh} + k_a + k_d \log d + k_f \log f - 9\log b \, , \tag{23}$$

where $b$ is the distance between the buildings along the signal path. $L_{bsh}$ and $k_a$ represent the increase of path loss due to a reduced base-station antenna height. Using the abbreviation

$$\Delta h_{Base} = h_{Base} - h_{Roof} , \tag{24}$$

where $h_{Base}$ is the base-station antenna height, we observe that $L_{bsh}$ and $k_a$ are given through

$$L_{bsh} = \begin{cases} -18\log(1 + \Delta h_{Base}) & h_{Base} > h_{Roof} \\ 0 & h_{Base} \le h_{Roof} \end{cases} , \tag{25}$$

$$k_a = \begin{cases} 54 & h_{Base} > h_{Roof} \\ 54 - 0.8\,\Delta h_{Base} & d \ge 0.5\text{ km and } h_{Base} \le h_{Roof} \\ 54 - 1.6\Delta h_{Base} d & d < 0.5\text{ km and } h_{Base} \le h_{Roof} \end{cases} . \tag{26}$$

The terms $k_d$ and $k_f$ control the dependence of the multi-screen diffraction loss as a function of distance, and the radio frequency of operation, respectively. They are given by

$$k_d = \begin{cases} 18 & h_{Base} > h_{Roof} \\ 18 - 15\dfrac{\Delta h_{Base}}{h_{Roof}} & h_{Base} \le h_{Roof} \end{cases} , \tag{27a}$$

and

$$k_f = -4 + 0.7\left(\frac{f}{925} - 1\right), \tag{27b}$$

for medium-sized cities and suburban centers with moderate tree densities; and by

$$k_f = -4 + 1.5\left(\frac{f}{925} - 1\right), \tag{27c}$$

for metropolitan centers.

This model is being considered for use by the International Telecommunication Union Radiocommunication Sector (ITU-R) in the International Mobile Telecommunications – 2000 (IMT-2000) standards activities. Some improved solutions for diffraction by multiple absorbing half-planes have also been developed [18, 19]. Other solutions, based on the Uniform Theory of Diffraction (UTD), are also available [20, 21]. The performance of the different methods in estimating the multiple-diffraction loss term and the final diffraction loss term is given in [22]. Recently, a correction to the COST-231-Walfisch-Ikegami Model has also been reported [23].

## 4.1.1.4 Dual-Slope Model

This model is based on a two-ray model [24, 25], which is used commonly when the transmitting antenna is several wavelengths or more above the horizontal ground plane. It is suitable for the line-of-sight (LOS) propagation regions. The propagation loss, $L(d)$, in this case is described by a dual-slope model. This can be represented as a function of $d$, the distance between the base station and the receiver. It is given by [26]

$$L(d) = L_b + \begin{cases} 10n_1\log d + P_1 & 1 < d < d_{brk} \\ 10(n_1 - n_2)\log d_{brk} + 10n_2\log d + P_1 & d \ge d_{brk} \end{cases} , \tag{28}$$

where $P_1 = PL(d_0)$, the path loss in dB at the reference point, $d_0$. $d_{brk}$ represents the breakpoint or the turning-point distance. The "point" where this transition occurs is often called the Fresnel breakpoint. $L_b$ is a basic transmission-loss parameter that depends on frequency and the antenna heights, and $n_1$ and $n_2$ represent the slopes of the best-fit line before and after the breakpoint. If the transmitter and receiver antenna heights are known, along with the distance between them, then the path loss can be computed, based on the two parameters $n_1$ and $n_2$. It is very reasonable to let $n_1 = 2$ for the region prior to the Fresnel breakpoint. There is much more variability in the path loss and the exponent for the region beyond the Fresnel breakpoint, with values of $n_2$ ranging from two to seven.

## 4.1.1.5 Other Models

Other models, including the use of wideband measurements for different situations, have been discussed in recent times [27, 28, 141]. These models have been developed from measurements, and use different parameters for different situations.

## 4.1.2 Indoor Case

Indoor radio propagation is not influenced by the terrain profile, as is outdoor propagation, but it can be affected by the layout in a building, especially if there are various building materials. The transmitted signal often reaches the receiver through more than one path, due to reflection, refraction, and diffraction of the radio wave by objects such as walls, windows, and doors inside a building.

**Table 2. The path loss measured in different buildings.**

| Building | $\gamma$ | PL (dB) | Frequency (MHz) | Ref. |
|---|---|---|---|---|
| Grocery store | 1.8 | 5.2 | 914 | [35] |
| Retail store | 2.2 | 8.7 | 914 | [35] |
| Open-plan Factories | 2.2 | 7.9 | 1300 | [36] |
| Open-plan Factories | 1.4-3.3 | – | 910 | [37] |
| Open-plan Factories B | 2.0 | 3.7 | 1300 | [38] |
| Open-plan Factories B | 2.1 | 4.0 | 1300 | [38] |
| Open-plan Factories C | 2.4 | 9.2 | 1300 | [38] |
| Open-plan Factories C | 2.1 | 9.7 | 1300 | [38] |
| Suburban office building open plan | 2.4 | 9.6 | 915 | [39] |
| Suburban office building open plan | 2.6 | 14.1 | 1900 | [39] |
| Suburban office building soft partition | 2.8 | 14.2 | 915 | [39] |
| Suburban office building soft partition | 3.8 | 12.7 | 1900 | [39] |
| Suburban office building hard partition | 3 | – | 850 | [40] |

**Table 3. The average floor attenuation factor (FAF).**

| Location | FAF (dB) | PL (dB) |
|---|---|---|
| **Office Building 1** | | |
| Through 1 floor | 12.9 | 7.0 |
| Through 2 floors | 18.7 | 2.8 |
| Through 3 floors | 24.4 | 1.7 |
| Through 4 floors | 27.0 | 1.5 |
| **Office Building 2** | | |
| Through 1 floor | 16.2 | 2.9 |
| Through 2 floors | 27.5 | 5.4 |
| Through 3 floors | 31.6 | 7.2 |

The distance/power model is the main propagation model for path loss. As shown in Equation (3), many researchers estimate the rate of decay of a transmitter signal through this relation [29-34]. In an enclosed environment, the value of $\gamma$ in Equation (3) may be 1.5 to 1.8 when the transmitter and receiver are placed in the same hallway and are in sight of each other. When the receiver is located within a room off the hallway, $\gamma$ ranges from three to four [30-33]. $\gamma$ also varies with frequency [33], and is dependent on the building materials used in a particular environment [34]. References [5] and [32] provide reviews of early work on these models. Table 2 [29] shows the parameters of Equation (3), determined by measurements for different buildings [35-40].

In order to take into account the attenuation due to walls and floors, two additional terms are added to Equation (3), resulting in [35, 41]

$$PL(d) = PL(d_0) + 10n \log(d/d_0) + \sum_{q=1}^{Q} FAF(q) + \sum_{p=1}^{P} WAF(p),$$

(29)

where $FAF(q)$ and $WAF(p)$ are the floor and the wall attenuation factors, respectively. Table 3 lists the $FAF$ values for two buildings [29, 30].

It is has been observed that the propagation path loss as a function of the distance also has two distinct regions for indoor environments [42], as described in Equation (29). When electromagnetic radiation is incident on a wall or a floor in an oblique fashion, less power will be transmitted through the wall than would occur at normal incidence. Reference [41] modifies the $WAF(p)$ term to $WAF(p)/\cos\phi_p$ and the $FAF(q)$ term to $FAF(q)/\cos\phi_q$, where $WAF(p)$ and $FAF(q)$ are the values of the attenuation factors at normal incidence, and $\phi_p$ and $\phi_q$ are the angles of incidence of the signal on the walls and floors, respectively. A diffraction term was also added to the formula in [41]. When the base station is out of the building, the path loss in the building was given in reference [43].

The empirical or statistical models described in this section are simple to implement, and are widely used when the accuracy of the data is not a critical requirement.

## 4.2 Site-Specific Models for Path Loss

Site-specific propagation models, also called deterministic models, are based on the theory of electromagnetic-wave propagation. Unlike statistical models, site-specific propagation models do not rely on extensive measurements, but on knowledge of greater detail of the environment, and they provide accurate predictions of the signal propagation.

In theory, the propagation characteristics of electromagnetic waves could be computed exactly by solving Maxwell's equations. Unfortunately, this approach requires very complex mathematical operations and requires considerable computing power. In reference [44], this method has been applied to simplified environments.

### 4.2.1 Ray-Tracing Technique

Ray tracing is a technique based on Geometrical Optics (GO) that can easily be applied as an approximate method for estimating the levels of high-frequency electromagnetic fields. GO assumes that energy can be considered to be radiated through infinitesimally small tubes, often called rays. These rays are normal to the surface of equal signal power. They lie along the direction of propagation and travel in straight lines, provided that the relative refractive index of the medium is constant. Therefore, signal propagation can be modeled via ray propagation. By using the

concept of ray tracing, rays can be launched from a transmitter location, and the interaction of the rays can be described using the well-known theory of refraction and reflection and interactions with the neighboring environment. In GO, only direct, reflected, and refracted rays are considered. Consequently, abrupt transition areas may occur, corresponding to the boundaries of the regions where these rays exist. The Geometrical Theory of Diffraction (GTD) and its uniform extension, the Uniform GTD (UTD) [45], complement the GO theory by introducing a new type of rays, known as the diffracted rays. The purpose of these rays is to remove the field discontinuities and to introduce proper field corrections, especially in the zero-field regions predicted by GO.

The Fermat principle and the principle of the local field are two basic concepts extensively used by the ray models. The Fermat principle states that a ray follows the shortest path from a source point to a field point, while the principle of the local field states that the high-frequency rays produce reflection, refraction, and diffraction when hitting a surface. This depends only on the electrical and geometrical properties of the scatterer in the immediate neighborhood of the point of interaction.

The ray-tracing method is widely used in propagation-model and system design [12, 42, 46-72, 145]. It is most accurate when the point of observation is many wavelengths away from the nearest scatterer. All scatterers are assumed to be large when compared to a wavelength. Two types of ray-tracing methods – the image method [12, 48, 55, 58] and the brute-force ray-tracing method – are generally used. These are now explained.

## 4.2.1.1 Image Method

This method generates the images of a source at all planes. These images then serve as secondary sources for the subsequent points of reflections. If there are $N$ reflecting planes, then there are $N$ first-order (i.e., one-reflection) images of a source, $N(N-1)$
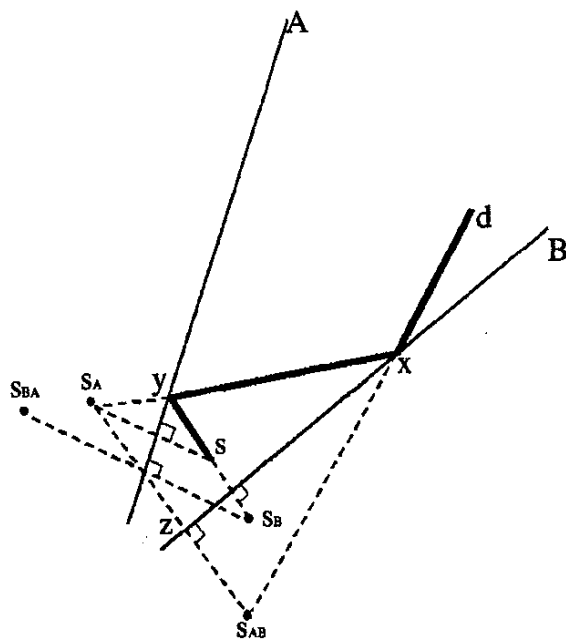
**Figure 3. Images due to a source placed between two mirrors, A and B.**
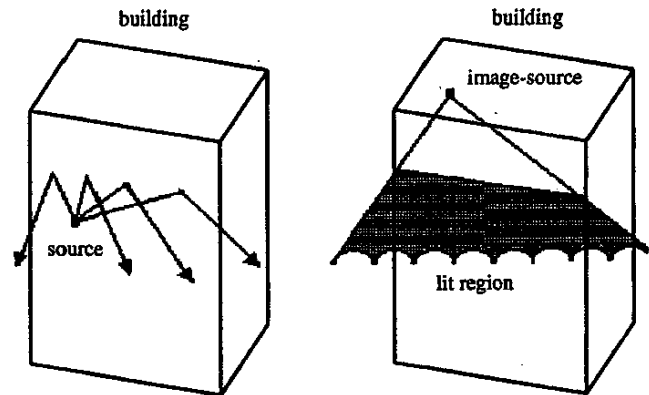
**Figure 4. The reflection by a wall in a building is modeled by an image source placed behind it and a lit region in front of it.**

two-reflection images, $N(N-1)(N-1)$ three-reflection images, and so on [48]. To determine whether an image of the source is visible at the destination is to trace the intersection of the reflected ray at all the necessary planes of interest. Thus, the energy reaches the destination through multiple reflections and contributes to the received power. Once a ray has been traced through all its reflections to the source, the attenuations associated with all the reflection terms are calculated.

The image method is efficient, but it can only handle simple environments. Many environments with which we are concerned in our daily life are complicated, and the conventional image method is not adequate. Figure 3 shows a source and its images, corresponding to two reflections [48]. The concept of a lit region has been introduced in [58] and is illustrated in Figure 4. An image is formed behind the cube representing a structure. This region where the image is formed is termed the unlit domain. For the two-dimensional case, only reflections from walls, and diffraction from corners in buildings, are taken into account. Ground reflections and rays over rooftops are neglected [58]. In references [53-55], a modified shooting-and-bouncing-ray technique, combined with the image method, has been used to deal with radio-wave propagation in furnished rooms. The effects of diffraction have also been considered. A threshold must be set with respect to the number and order of reflection and diffraction rays that can be considered.

## 4.2.1.2 Brute-Force Ray-Tracing Method

This method considers a bundle of transmitted rays that may or may not reach the receiver. The number of rays considered and the distance from the transmitter to the receiver location determines the available spatial resolution and, hence, the accuracy of the model. This method requires more computing power than the image method.

A finite sample of the possible directions of the propagation from the transmitter is chosen. A ray is launched for each such direction. If a ray hits an object, then a reflecting ray and a refracting ray are generated. If a ray hits a wedge, then a family of diffracting rays is generated. A reception sphere with the correct radius can describe a region that will receive exactly one ray. If the radius is too large, two rays could be received, and the same specular ray might be counted twice. If the radius is too small, it is possible that none of the rays will reach the reception sphere, and
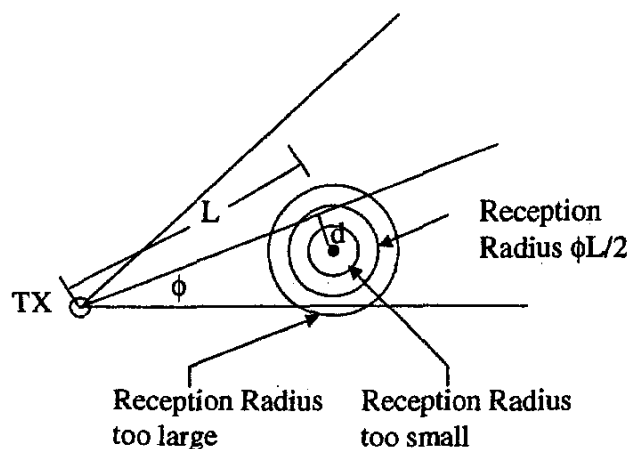
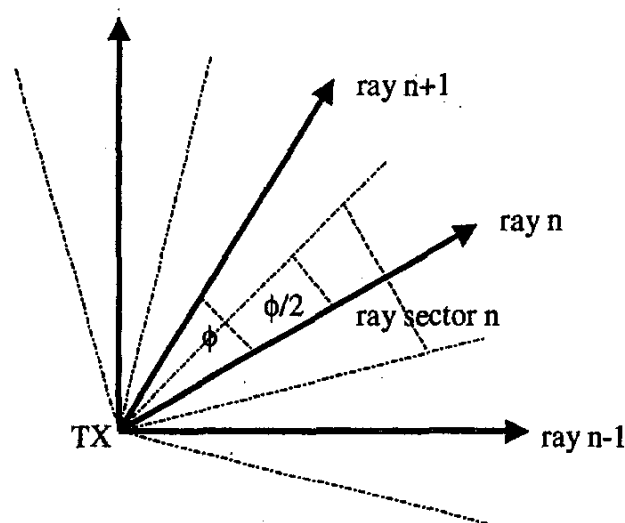**Figure 5. The reception sphere for a two-dimensional ray tracing.**



**Figure 6. Rays generated from a source in two dimensions.**

the specular ray will be excluded [42, 59]. Figure 5 shows the proper size of the reception sphere that may receive a ray. For each receiver location, the perpendicular distance, $d$, from the receiver to the ray is computed, together with the total (unfolded) ray-path length, $L$, from the source to the perpendicular projection point. If $d$ is greater than or equal to $(\phi L)/2$ for the two-dimensional case, or $(\phi L)/\sqrt{3}$ for the three-dimensional case, the ray is treated as not having reached the receiver location. Here, $\phi$ is the angle between two rays. Otherwise, the ray is considered to contribute to the received signal. There is no reception sphere associated with the usage of the image method.

The key part of the ray-tracing method is the generation and description of the rays. There are two kinds of methods to obtain the rays at the source point. One is a two-dimensional (2D) approach; the other is a three-dimensional (3D) method.

**Two-dimensional ray-tracing model [42].** In two dimensions, all the rays or ray tubes are ray sectors, as shown in Figure 6. At the source, rays are launched along different direc-

tions with the same sector angle, $\phi$, in a plane. How the angle $\phi$ is chosen depends on the accuracy required and the computation time. If the angle is small, it will provide high accuracy and it will take a lot of time to compute. For example, if the angle $\phi = 1°$, then there will be 360 rays to be traced.

Each ray is launched from the source, and can be traced through a binary tree. An intersection with a surface of an object is represented by a node in the tree. The incident ray is decomposed into an object-reflected ray and an object-penetrated ray. It is assumed that the reflected ray propagates along the specular direction (the incidence angle equals the aspect angle), and that the ray that penetrates the object keeps the original direction of the incident ray. Both rays then propagate to the next intersection. An intersection with a wedge is also represented by a node, and the diffraction point is processed as a source, and a large number of rays must be launched. The decomposition process is repeated as a recursion process. This procedure is continued until the rays are weaker than an assumed threshold, or until the ray leaves a predefined propagation area, or until the ray is received. The strength of the field at the receiver is then calculated according to Equation (9).

A two-dimensional diffraction model was introduced in [62, 64]. The authors considered the various buildings to be vertical knife edges, neglecting the over-rooftop diffraction and ground reflection. Because the buildings were much higher than the base-station (BS) and mobile-station (MS) antennas in an urban microcellular environment, the weak contribution from the signals from the over-rooftop rays could be neglected. No rays due to a single ground reflection from the transmitter to the receiver existed in the shadow regions. For ranges less than 1 km from the transmitter (primary source), the received power could have a range $(R)$ dependence given by a power law of $1/R^2$. However, for LOS regions, the ground reflections appeared to be less important.

As reported in [64], the two-dimensional ray-tracing algorithm is quite accurate when the transmitting and receiving antenna heights are significantly below the rooftops of the surrounding buildings. This model of propagation between a transmitter and receiver located close to the ground is usually called the canyon model.

When using a two-dimensional model, the inputs are: a) the two-dimensional geometry described by means of vectors specifying the location of the building walls; b) the estimated electrical characteristics of the building walls (the permittivity and conductivity, or the scalar reflection coefficient); c) the base-station location; d) the antenna patterns; and e) the frequency of operation.

**Three-dimensional ray-tracing model [12, 64-72].** The transmitter and receiver are modeled as point sources when using this ray-tracing technique. In order to determine all possible rays that may leave the transmitter and arrive at the receiver in three dimensions, it is necessary to consider all possible angles of departure and arrival at the transmitter and receiver. Rays are launched from the transmitter at an elevation angle $\theta$ and with an azimuth angle $\phi$, as defined in the usual coordinate system. Antenna patterns are incorporated to include the effects of antenna beamwidth in both azimuth and elevation.

To keep all the ray-manipulation routines general, it is desirable that each ray tube occupy the same solid angle, $d\Omega$, and that each wavefront have an identical shape and size at a distance $r$ from the transmitter. Additionally, these wavefronts must be such that they can be subdivided, so that an increased ray resolution can

be easily handled. For example, let $r = 1$, and let the total wavefront be the surface of a unit sphere. The problem then becomes one of subdividing the sphere's surface into areas of equal "patches," so that all are of the same size and shape and so that, collectively, they cover the surface of interest without gaps. Hexagonal [12] and triangular [53, 54] ray wavefronts have also been used.

The procedure of ray tracing in three dimensions is similar to a two-dimensional model, but more computational time is needed.

Some sectors of the walls in a corridor can be made of different materials, for example, wood, metal, concrete, or even glass, which may have different reflectivities for the incident wave. Neglecting the differences among the reflectivities of the various materials will degrade the prediction accuracy of the propagation model. Therefore, in [12] the concept of an "effective building material" was proposed to represent the complicated physical constitutive materials used in the walls of a building. However, the permittivity of this effective material is not easy to determine, since it depends on experimental data as well as on the propagation model. To simplify this problem, patches of different dielectric constants and physical sizes were introduced in [65]. It is noted that the size and dielectric constant of each patch were chosen according to the physical dimensions and the material of which it was made.

The key to a propagation model based on ray-tracing is to find a computationally fast way to determine the dominant ray paths so as to provide accurate path-loss predictions. It is well known that for outdoor propagation prediction, diffraction from edges must be accounted for in addition to specular reflections, especially in non-LOS regions. Unfortunately, diffraction is very time consuming to model, since a single incident ray encountering an edge will generate a whole family of new rays. The generation of a large number of diffracted rays limits the number of diffractions that can be considered. For any given path, we choose at most two, unless an approximation can be made to find the important contributing rays. In order to find the contributing rays in an urban environment, where the building walls are nearly always vertical planar polygons, a vertical-plane-launch (VPL) method has been developed [66]. The vertical-plane-launch approach accounts for specular reflections from vertical surfaces and for diffraction at the vertical edges, and approximates diffraction along horizontal edges by restricting the diffracted rays to lie in the plane of incidence or in the plane of reflection. The vertical-plane-launch approach can treat many multiple forward diffractions at horizontal edges. It can also be used for rooftop antennas, and for areas where buildings of different heights exist.

To improve the efficiency of ray-tracing models, many researchers have developed a large number of methods [68, 72]. In [68], a hybrid technique was presented, where the object database was held in two dimensions, but a ray-tracing engine operated in three dimensions. The three-dimensional rays were produced by combining the results of two two-dimensional ray tracers, one on a horizontal plane and the other on a vertical plane. Moreover, by significantly enhancing the concept of "illumination zones," the performance of the algorithm could be dramatically improved.

A comparison between a two-dimensional model and a three-dimensional model was made in [64].

## 4.2.2 FDTD Models

Based on Geometrical Optics (GO) and usually supplemented by UTD, a ray-tracing algorithm provides a relatively simple solution for radio propagation. However, it is well known that GO provides good results for electrically large objects, and UTD is rigorous only for perfectly conducting wedges. For complex lossy structures with finite dimensions, ray-tracing fails to correctly predict the scattered fields. In a complicated communication environment, transmitting and receiving antennas are often inevitably installed close to structures with complex material properties for which no asymptotic solutions are available. Such problems can be solved by numerical solution of Maxwell's equations. In particular, the Finite-Difference Time-Domain (FDTD) method is an alternative. The advantages of the FDTD method are its accuracy, and that it simultaneously provides a complete solution for all the points in the map, which can give signal-coverage information throughout a given area.

In a simple outdoor environment, a two-dimensional FDTD is generally applied [73]. A simple approach for introducing the correct spherical-wave spreading has been developed. A comparison with FDTD predictions could be used to evaluate and refine the GTD-based methods.

A reduced formulation for the standard FDTD technique [74] – requiring four scalar field components instead of the usual six – was used to predict channel statistics inside a residential building. Measurements were also conducted, and the results were compared with simulated data. In order to introduce arbitrarily shaped antennas into the simulations, a two-and-one-half dimension (2.5D) or a multi-mode FDTD method was established for indoor radio-propagation calculations [75].

A hybrid technique [76], based on combining a ray-tracing method with an FDTD method, for more accurate modeling of radio-wave propagation was also suggested. The basic idea was to use ray tracing to analyze wide areas, and the FDTD to study areas close to a structure with complex material properties, where ray-based solutions are not sufficiently accurate.

As a numerical method, the FDTD requires large amounts of computer memory to keep track of the solution at all locations, and extensive calculations to update the solution at successive instants of time. The application of an accurate numerical-analysis method to model an entire area is neither practical (because of the computational resources required) nor is it necessary for open areas without many objects.

## 4.2.3 Moment-Method Models

Ray-tracing models can be used with sufficient precision to predict radio coverage for large buildings having a large number of walls between the transmitter and the receiver, while the Method of Moments (MoM) model is better when higher precision is required and when the size of the buildings is smaller. A combination of these two models is also possible, using the advantages of each of them. For cases where a lot of small but dominant obstacles are present, or where there are paths that cannot be taken into

account by a ray-tracing model, the MoM model can be used [77, 78].

The solutions determined by the MoM are numerically exact as long as the spatial segmentation used for the objects is small enough. Due to limitations of computer memory and CPU time, the MoM is usually applied for analyzing objects that are tens of wavelengths in size. However, by choosing structures with dimensions around a few wavelengths, the MoM can be used to check and verify a ray-tracing program. A two-dimensional problem that included stair-shaped walls above a lossy ground was simulated by using both the MoM and the ray-tracing method [77].

The transmission of a UHF wave through a window in a wall is critical when integrating systems that include both indoor and outdoor areas. A novel simulation approach, based on the Moment Method, was presented in [79]. In the simulations, the walls were modeled as two long dielectric slabs, long enough so that any diffraction or reflection at the outer edges would not influence the results. No distinction was made between the concrete and the brick parts of the walls. The glass plates were also assumed to be homogeneous, and the aluminum frame was modeled as a perfectly conducting material. The resulting simulations were then compared to a set of measurements, where good agreement was achieved.

A hybrid approach, combining the ray-tracing method and the Periodic Moment Method (PMM) for material objects, was developed to study indoor wave propagation, penetrations, and also scattering due to periodic structures in buildings [80]. The PMM was applied to evaluate the specular and grating transmission and reflection coefficients of the periodic structures. Those data were then used in a ray-tracing program to find the specular and grating rays for each ray tube illuminating one of the periodic structures. Those excited ray tubes were continuously traced to determine their contributions to the receiving antennas.

## 4.2.4 Artificial Neural-Network Models

The main problem with the statistical models is usually the accuracy, while the site-specific models lack computational efficiency. The use of artificial neural networks (ANNs) has shown very good performance in solving problems with mild nonlinearities on a set of noisy data. This case corresponds to a problem of field-level prediction, as the data obtained from measurements is always noisy. Another key feature of the neural network is the intrinsic parallelism, allowing for fast evaluation of the solutions.

The ANN model [81] that had the form of a multilayer perception was generally used with 12 inputs and one output. It was developed to predict the propagation in an indoor environment. In this case, a two-dimensional floor plan was used for a database with a resolution of 10×10 cm. All particular locations were classified into 11 distinct categories, such as wall, corridor, outdoor area, laboratory, and so on. One input of the network represented the normalized distance from the transmitter to the receiver. In addition, there was an input for each defined environmental category. Other inputs represented either a normalized number of occurrences (doors and windows), or an appropriate percentage (wall, corridor, and so on) of that category along the straight line drawn from the transmitter to the receiver. The process of learning may have lasted for a couple of hours, but the process for field-level prediction was fast. The accuracy of such a prediction model depends significantly on the accuracy of the environmental databases.

In [82], theoretical investigations into the suitability of a neural-network simulator for the prediction of field strength, based on topographical and morphographical data, were presented. Effective input and output data processing was developed using deterministic and heuristic formulas for the training of a neural-network simulator. The network used was similar to that described in [81]. The inputs were the frequency, the heights of the antenna for the base and mobile stations, respectively, and the distances between them. The output was the field strength.

Although the multilayer neural network [82] is a useful method for approximating the propagation loss, it however suffers from the drawbacks of slow convergence and unpredictable solutions during learning. To overcome these difficulties, radial-basis function (RBF) neural networks that have a "linear-in-the-parameters" representation were proposed to enhance the real-time learning capabilities and to achieve rapid convergence [83]. The RBF neural network is a two-layer localized receptive field network, the output nodes of which form a combination of radial activation functions computed by the hidden-layer nodes. Appropriate centers and connection weights in the RBF network lead to a network that is capable of forming the best approximation to any continuous nonlinear mapping, up to an arbitrary resolution. Such an approximation introduces a best-nonlinear-approximation capability into the prediction model, in order to accurately estimate the propagation loss over an arbitrary environment, based on adaptive learning from measurement data. Okumura's data are often included to demonstrate the effectiveness of the RBF neural-network approach.

## 4.2.5 Other Models

Recently, many new methods have been introduced to predict propagation for mobile communications. Some of these are described in the following subparagraphs.

## 4.2.5.1 Vector Parabolic-Equation Model

This model has been applied to the modeling of radiowave propagation in an urban environment. As a parabolic version of Maxwell's equations, it allows a full treatment [84, 138, 139] of three-dimensional electromagnetic scattering, which is not possible with scalar versions of the algorithm. It is particularly useful for accurate modeling of scattering by a single building or by a group of buildings at microwave frequencies. Examples include scattering by a building with a hemispherical roof, and scattering by a group of buildings with sloping roofs.

## 4.2.5.2 Fast Far-Field Approximation Model

This model is substantially faster than conventional integral-equation- (IE-) based techniques. The technique is improved by incorporating the Green's-function perturbation method. The method has been applied to gently undulating terrains, and compared with published experimental results in the 900 MHz band. It has also been successfully applied to more hilly terrain, and to surfaces with added buildings [85]. An improved version of the "shifting function" has been introduced, which can improve the

performance of the technique for more-challenging problems, such as scattering from a wedge. The issues of profile truncation and small-scale-roughness effects have been addressed, and the numerical results presented showed excellent agreement with published measured data.

### 4.2.5.3 Waveguide Model

In large metropolitan areas that have tall buildings, the transmitting and receiving antennas are both located below the rooftops, and the city streets act as a type of wave-guiding structure for the propagating signal [86, 87, 140]. In this case, there is a need to develop efficient algorithms for the computation and mapping of the field distribution in such structures. Theoretical analysis of propagation in a city street modeled as a three-dimensional multi-slit waveguide was proposed. Assuming the screens and slits are distributed by a Poisson law, the statistical propagation characteristics in such a waveguide are expressed in terms of multiple ray fields approaching the observer. Algorithms for the path-loss prediction were presented and compared with experimental data in the references cited above.

### 4.2.5.4 Boltzmann Model

This model was initially developed for simulated fluid flows. It describes a physical system in terms of the motion of fictitious microscopic particles on a lattice [88, 143]. This technique can take into account complicated boundary conditions. Two-dimensional simulations were performed, starting from a city map, and a renormalization scheme was proposed. The method, which is simple and easy to implement, provided good path-loss predictions when compared with site measurements.

### 4.3 Summary of Models for Path Loss

A summary of the various propagation models dealing with path loss has been given. A brief comparison of some of the main models is presented in Table 4. Propagation models dealing with path loss for mobile communication have been emphasized, using two very different approaches. First, a simple empirical or statistical model of the path loss was considered, where some of the parameters used were determined empirically from measurements. The second approach used site-specific methods. Ray tracing was the main method. Some other numerical methods used in electromagnetic-field computation have also been applied.

Each of these two kinds of approaches makes a very different trade-off of accuracy versus complexity. The empirical (statistical) models are extremely simple (no environmental information is used, other than in the choice of the parameters), but the predictions are not very accurate. On the other hand, site-specific models are considerably more accurate than the empirical models, but they require a great deal of specific information about the area of interest (at a minimum, the locations of all the objects, and possibly the locations of large objects).

### 4.4 Efficient Computational Methods For Propagation Prediction for Indoor Wireless Communication

This section presents two different deterministic methods for efficient characterization of an indoor channel. First, an improved version of a ray-tracing method is presented. Next, the FDTD method is used to calculate the effects of walls in an indoor wave-propagation environment.

Table 4. A comparison of various models for path loss.

| Model Name | Suitable Environment | Complexity | Experimental Data | Details of Environment | Accuracy | Time | Other |
|---|---|---|---|---|---|---|---|
| Okumura Model | Macrocell | Simple | Based on experiments | No | Good | Little | Graphical path-loss data |
| Hata Model | Macrocell (early cellular) | Simple | No | No | Good | Little | |
| COST-231 | Microcell (outdoor) | Simple | No | No | Good | Little | |
| Dual-Slope | Microcell and picocell (LOS region) | Simple | No | No | Good | Little | |
| Ray-Tracing | Outdoor and indoor | Complex | No | Yes | Very Good | Very Much | |
| FDTD | Indoor (small) | Complex | No | Every detail | Best | Very Much | Often combined with ray tracing |
| MoM | Indoor (small) | Complex | No | Every detail | Best | Very Much | |
| ANN | Outdoor and indoor | Complex | Yes | Detail | Very Good | Little | Takes time to learn from experimental data |
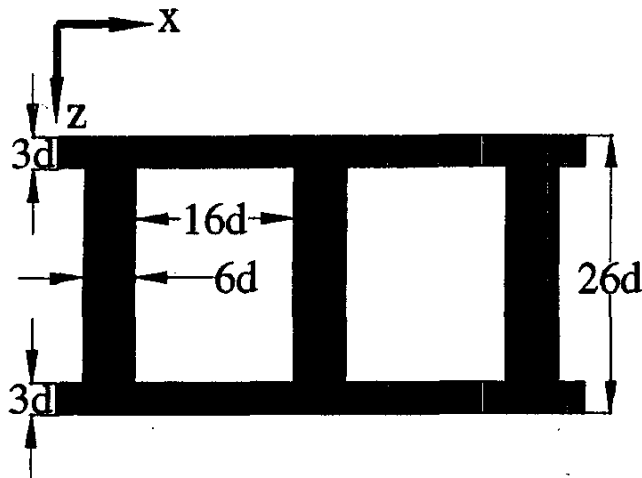
Figure 7. A typical periodic inner structure of walls.

## 4.4.1 Efficient Ray-Tracing Methods

The application of several ray-tracing techniques in combination with the Uniform Theory of Diffraction has been an efficient method for the prediction of propagation in the UHF (communication) band in an indoor environment. This is discussed in detail [136], where the computational efficiency of the two-dimensional ray-tracing method was improved by reorganizing the objects in an indoor environment into irregular cells. In addition, by making use of the two-dimensional ray-tracing results, a new three-dimensional propagation-prediction model was developed that can save 99% of the computational time of a traditional three-dimensional model. This new hybrid model is more accurate than two-dimensional models and more efficient than traditional three-dimensional models in computing the path loss to any point in a building. In this model, reflection and refraction by layered materials and diffraction from the corners of walls was considered. This theoretical model had a good correlation with experimental data.

## 4.4.2 Analysis of the Effects of Walls on Indoor Wave Propagation Using FDTD

The ray-tracing technique does not take the effects of the inner structure of walls into account for indoor propagation prediction. A numerical approach to treat this problem, using the FDTD method, is now described. Numerical results for the path loss calculated by an FDTD method were compared with those obtained by the ray-tracing technique. The application of ray-tracing techniques in propagation prediction has been under development for more than a decade. They are powerful and easy to use. There have been a number of recent investigations into indoor radio-propagation modeling using the ray-tracing method [57, 65, 126], but few have paid attention to the inner structure of the walls [134, 135]. When using a ray-tracing method, it is assumed that reflection from walls has a substantial specular component. Typical concrete blocks used in wall construction are shown in Figure 7. The air hole in the block forms a periodicity in the blocks. It has been found that non-specular reflection occurs when the operating frequency is above 1.2 GHz [134]. In this approach, the reflection and transmission characteristics of the walls can be derived by solving for higher-order Floquet modes. Also, the

method of homogenization can be used to determine the effective material properties of walls, but they did not consider non-specular reflection.

The FDTD method was used to predict propagation properties for indoor environments [137]. The periodic structure of walls was also considered. Numerical results for the path loss were calculated by an FDTD method, and were compared to those obtained by the ray-tracing method. It was proved that the inner structure of the walls had a considerable influence on the path loss when predicting propagation, and that the FDTD method can give more accurate results.

## 4.4.2.1 Numerical Results

The fields of the environment were calculated using a two-dimensional FDTD method when the wall was first assumed to be a periodic structure, and then uniform in nature, with an effective dielectric constant. For the FDTD method, 5000 time steps were calculated, and it took more than six hours of CPU time on a PC. A two-dimensional ray-tracing method was used to analyze the uniform structure, and it took only 10 minutes to compute the path loss for 250 sample points.

Figure 8 shows the simulation results of the path loss for the sample points. This indicates that the effects of the inner structure of the walls cannot be neglected for propagation prediction. The maximum difference in the field strength when the wave was assumed to propagate through a periodic structure and through a uniform structure was more than 10 dB when using the FDTD method. As a full-wave analysis tool, the FDTD is more accurate than the ray-tracing method. All the propagation phenomena, such as reflection, transmission, and diffraction, are included. A ray-tracing method considers only reflection and transmission. The maximum difference in the field strength when propagating
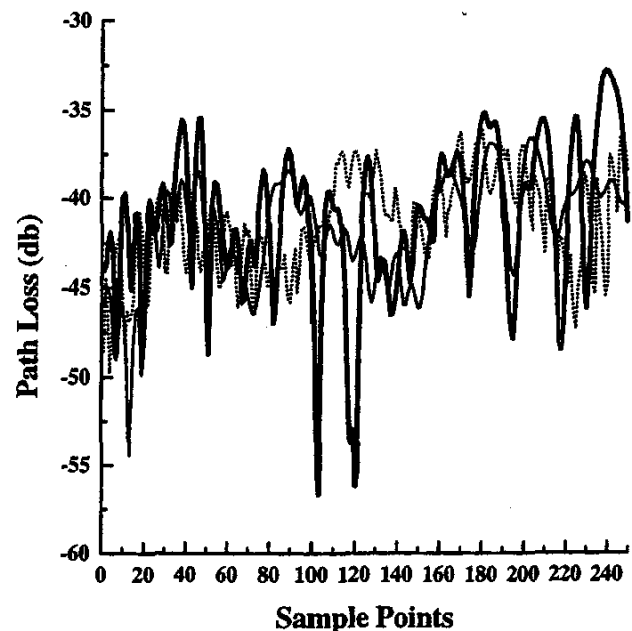


Figure 8. Simulation results using three different FDTD methods: ——FDTD (periodic); —— FDTD (uniform); - - - - Ray tracing (uniform).

through a periodic structure using the FDTD method and the ray-tracing method was around 18 dB.

# 5. Models For Small-Scale Fading

Small-scale fading refers to the dramatic changes in the signal amplitude and phase that can be experienced as a result of small changes (as small as a half wavelength) in the spatial separation between a receiver and a transmitter. These dramatic changes in the envelope of the received signal are described statistically by a stochastic process.

In order to get a sound understanding of the channel, it is important to study the distribution of the envelope of the received signal. A few possible choices of the statistical distributions for modeling the envelope are explained below. As explained and emphasized in [160], we have to be extremely careful when using a statistical model, as a complete lack of knowledge of the system cannot be supplemented by a stochastic distribution.

## 5.1 Ricean Distribution

This is also called a Rice distribution or a Rician distribution. When there is a dominant stationary (non-fading) signal component present, such as a line-of-sight propagation path, the fading distribution is Ricean. The Ricean distribution is given by

$$p(r) \begin{cases} \dfrac{r}{\sigma}\exp\left[-\dfrac{r^2+A^2}{2\sigma^2}\right]I_0\left(\dfrac{Ar}{\sigma^2}\right) & A \geq 0, r \geq 0 \\ 0 & r < 0 \end{cases} \quad (30)$$

where $r$ is the amplitude of the envelope of the received signal, and $2\sigma^2$ is the predicted mean power of the multipath signal. $A$ denotes the peak amplitude of the dominant signal, and $I_0(\bullet)$ is the modified Bessel function of the first kind and zero order. The Ricean distribution is often described in terms of a parameter, $K$, which is defined as the ratio between the deterministic signal power and the variance of the multipath. It is given by [10]

$$K(\text{dB}) = 10\log\dfrac{A^2}{2\sigma^2}. \quad (31)$$

$K$ is known as the Ricean factor, and completely specifies the distribution.

It is possible to estimate the Ricean $K$ factor of a signal from measurements of received power versus time. One approach is to compute the distributions of the measured data and to then compare the result to a set of hypothesis distributions, using a suitable goodness-of-fit test. Another is to compute a maximum-likelihood estimate using an expectation/maximization (EM) algorithm. However, both of these approaches are relatively cumbersome and time consuming. A simple and rapid method has been developed, based on calculating the first and second moments of the time-series data. The method is exact when perfect moment estimates of the Ricean envelopes are available. In that case, the factor $K$ can only be obtained implicitly by equating a ratio of the measured moments to a complicated function of $K$. By contrast, the method described in [89] yields an explicit and quite simple expression for $K$ in terms of the measured moments.

## 5.2 Rayleigh Distribution

As the dominant signal in a Rician distribution becomes weaker, the composite signal resembles a noise signal that has an envelope of a Rayleigh distribution. For mobile-radio channels, the Rayleigh distribution is widely used to describe the statistical time-varying nature of the received envelope of a flat-fading signal, or of an individual multipath component. The Rayleigh distribution has a probability density function (PDF) given by

$$p(r) = \begin{cases} \dfrac{r}{\sigma^2}\exp\left(-\dfrac{r^2}{2\sigma^2}\right) & 0 \leq r \leq \infty \\ 0 & r < 0 \end{cases}. \quad (32)$$

The probability that the envelope of the received signal does not exceed a specified value $R$ is given by the corresponding cumulative distribution function (CDF):

$$P(R) = P_r(r < R) = \int_0^R p(r)dr = 1 - \exp\left(-\dfrac{R^2}{2\sigma^2}\right), \quad (33)$$

where $r$ is the envelope amplitude of the received signal, and $2\sigma^2$ is the predicted mean power of the multipath signal.

Since the fading data are usually measured in terms of the fields, quantities for a particular distribution cannot be assumed. The median value is often used rather than the mean values, and it is easy to compare different fading distributions, which may have widely varying means. A typical Rayleigh fading envelope for a moving mobile at 900 MHz is shown in Figure 9 [90].

## 5.3 Log-Normal Fading Model

This model is used to quantify the distribution of rays that experience multiple reflections and diffractions between a transmitter and a receiver. The log-normal PDF can be expressed as

$$p(r) = \dfrac{1}{r\sqrt{2\pi\sigma^2}}\exp\left\{-\dfrac{[\ln(r)-m]^2}{2\sigma^2}\right\}, \quad (34)$$
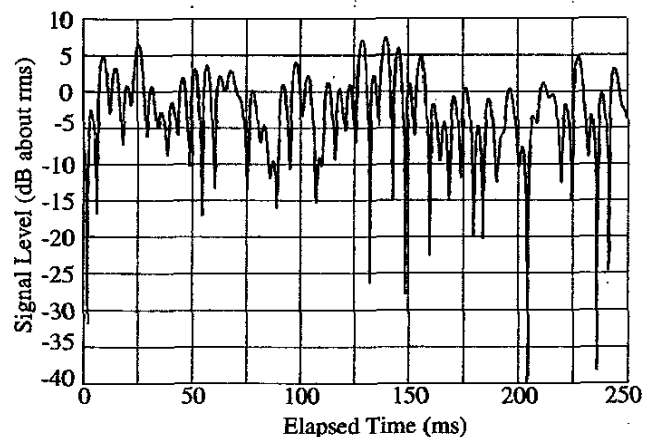


Figure 9. A typical Rayleigh fading envelope at 900 MHz, received by a mobile unit traveling at 120 km/hr.

where $m$ is the median value, and $\sigma$ is the standard deviation of the corresponding normal distribution, obtained by using the transformation $y = \ln(r)$ [91]. Techniques such as the Monte Carlo method and the Schwartz and Yeh method have been developed to simulate the power sum for the log-normal components [92].

## 5.4 Suzuki Model

The Suzuki model combines two distributions, comprised of the log-normal and Rayleigh distributions. It provides a more-accurate approximation of the sum of correlated complex log-normals for a wider variety of channel behaviors. Usually, the Rayleigh distribution is obtained from two statistically independent normal processes, $\mu_1(t)$ and $\mu_2(t)$, with zero means and identical autocorrelation functions, according to the relation

$$\xi(t) = \sqrt{\mu_1^2(t) + \mu_2^2(t)}, \qquad (35)$$

where $\xi(t)$ can be regarded as the envelope of one complex-valued normal random process, $\lambda(t)$. The requirement of statistical independence between $\mu_1(t)$ and $\mu_2(t)$ is identical to the demand for a symmetrical power spectrum for $\lambda(t)$. The received power, averaged over a period of few seconds, can vary considerably, due to various shadowing effects. In order to adapt the model to this behavior, the process $\xi(t)$ is substituted for by the product $\eta(t) = \zeta(t) \cdot \xi(r)$, where the log-normal process $\zeta(t) = \exp[\mu_3(t)]$ is defined by a normal process $\mu_3(t)$, with variance $s^2$ and mean $m$. The product process with this particular amplitude-density distribution is called the Suzuki process, and is given by [93]

$$p_\eta(r) = \int_0^\infty \frac{r}{\sigma^2} \exp\left(-\frac{r^2}{2\sigma^2}\right) \frac{1}{\sqrt{2\pi} s\sigma} \exp\left[-\frac{(\ln\sigma - m)^2}{2s^2}\right] d\sigma, \quad (36)$$

where $\sigma$ is the standard deviation and $r$ is the amplitude. The assumption of statistical independence does not always meet the real conditions in multipath wave propagation, so it has been modified [94], and was simulated in [95].

This is a widely accepted statistical model for the received-signal envelope in macrocellular mobile radio channels where there is no direct LOS path.

## 5.5 Nakagami Model

The Nakagami model was developed in the early 1940s by Nakagami. The corresponding probability density function is written as [96]

$$p(r) = \frac{2m^m r^{2m-1} \exp\left(-\frac{m}{\Omega} r^2\right)}{\Gamma(m)\Omega^m}. \qquad (37)$$

Here, $r$ is the envelope amplitude of the received signal. $\Omega = \langle r^2 \rangle$ is the time-averaged power of the received signal, and

$m = \langle r^2 \rangle^2 / \langle (r^2 - \langle r \rangle^2)^2 \rangle$ is the inverse of the normalized variance of $r^2$. $\Gamma(\bullet)$ is the Gamma function. The Nakagami PDF may be shown to be a more-general expression of other well-known density functions. The Rayleigh probability density function is obtained for $m = 1$. The Nakagami PDF can also be approximated by both Rice and lognormal distributions over certain domains, given appropriate bounds on the parameters.

A Nakagami model, parameterized by the fading severity parameter, $m$, has been shown to fit well to some urban multipath propagation data. A simulation of the Nakagami model has been presented in [97].

## 5.6 Weibull Model

This model arises when results from mobile-radio propagation measurements are plotted on graph paper that is scaled such that a Rayleigh distribution appears as a straight line with a slope of $-1$. The Weibull PDF can be written as [91]

$$p(r) = \frac{\alpha b}{r_0}\left(\frac{br}{r_0}\right)^{\alpha-1} \exp\left[-\left(\frac{br}{r_0}\right)^\alpha\right], \qquad (38)$$

where $\alpha$ is a shape parameter that is chosen so as to yield a best fit to the measured results. Here, $r_0$ is the RMS value for $r$, and $b = \left[(2/\alpha)\Gamma(2/\alpha)\right]^{1/2}$ is a normalization factor. For the special case in which $\alpha = 1/2$, the Weibull PDF becomes a Rayleigh PDF. The Weibull distribution provides flexibility to model any shape offered by a Nakagami distribution, but it lacks a theoretical basis. It was shown that the Weibull distribution characterizes indoor propagation-path losses quite well in [146].

## 5.7 Other Fading Models

Many other models for fading have been developed. Some of these are the Rice Log-Normal Model [98], the Nakagam-Rice Model [99], the Nakagami Log-Normal Model [100], and the K-distribution, which is a substitute for the Rayleigh log-normal distribution [101]. These are mixtures of two kinds of distributions, and are now widely used. In [102], propagation models that include both the effects of shadowing and multipath fading were developed and used in studying terrestrial and satellite channels. In [103] and [104], a new theoretical model for the prediction of fast fading in an indoor environment was developed. This model made the assumption that the number of dominant propagation paths that contribute to the signal in the receiver in a multipath environment is not infinite, but rather small (e.g., 15). This assumption led to the development of a new theoretical model, called "POCA," that is more general and more efficient than the Rayleigh Model, especially for indoor environments. It is generally fit for environments in which there exists a small number of dominant propagation paths.

In this section, some of the statistical models for fading have been introduced. Only their PDF distributions have been described. Details of the implementations of these models can be obtained from the various references cited.

# 6. Impulse-Response Models

The narrowband or continuous-wave (CW) path loss is a parameter that can predict the power level of the system and the space coverage of a base station. In modern mobile-communication systems, with high data rates and small cell sizes, it is necessary to model the effects of multipath delay, as well as modeling fading. The impulse response is a useful characterization of the system, since the output of the system can be computed through convolution of the input with the impulse response, if the system is linear. A multipath propagation channel is modeled as a linear filter, and has a complex baseband impulse response [105-125, 144, 147-151].

In digital wireless communications, one of the main reasons for the occurrence of bit errors is inter-symbol interference (ISI) caused by multipath propagation. If the symbol rate is much lower than the coherent bandwidth, the time-delay spread can be neglected. In this case, multipath propagation only causes fading of the signal level, and Gaussian noise is the dominant factor that causes bit errors. If the symbol rate is relatively high, the time-delay spread cannot be neglected.

A large number of measurements have been made for the impulse response, both for outdoor and indoor environments. Some models have been derived based on the measured data. The results of measurements, along with some typical models, are described here, followed by a description of some deterministic models.

## 6.1 Models Based on Measurement Results

Because of the importance of determining the time-delay spread for wireless communications, a number of wideband channel-sounding techniques have been developed. These techniques may be classified as

A. Direct pulse measurements;
B. Spread-spectrum sliding correlator measurements; and
C. Swept-frequency measurements.

The block diagram for each of these techniques is shown in Figure 10 [10]. Almost the same results can be obtained from the last two methods [105]. Some measurements for both indoor and outdoor environments, and the calculated RMS time delays have been summarized in Table 5. In this table, "Med" indicates median values, "T-R" indicates the distance between the transmitter and receiver, and "Ave" implies the mean average values. In Table 5, it is found that the RMS delay spread varies from several nanoseconds to several microseconds, corresponding to different environments and frequencies.

There are many factors affecting the impulse response, such as the frequency, the height of the transmitting and receiving antennas, fixed objects (mountains, buildings, or indoor furniture), and moving humans or objects close to the transmitter and/or the receiver. It is shown in Table 5 that the RMS time delay varies little for different frequencies for indoor environments [106], but a different conclusion was obtained in [107]. In [108], it was found that at 11.5 GHz, the RMS time delay in most cases was significantly smaller than at 2.4 GHz and 4.75 GHz, for which the values were, in general, about the same. The reason that two different conclusions were reached is that all of these various conjectures have been derived from specific measurements. Obstructed line-of-

sight (OLOS) channels are subject to higher variations in RMS delay spread, caused by movement of the terminal around a small area, because of the presence of a larger number of scatters in the obstructed line-of-sight environment than in the LOS environment. On the other hand, the short-time variations in the RMS delay spread in obstructed line-of-sight environments were found to be less than those in LOS environments [117]. It is concluded that in an empty indoor environment, the RMS delay spread is a function of the transmitter-receiver separation. When there is furniture and mazes of semi-permanent partitions, the RMS delay spread becomes constant for all ranges [105]. It was shown in [121] that in many cities where the terrain is flat, the RMS delay spreads do not exceed 7 or 8 µs, and that in urban areas with surrounding hills, the RMS delay spreads do not exceed 13.5 µs. In [26, 123], the RMS delay spread was analyzed as a function of the path loss and
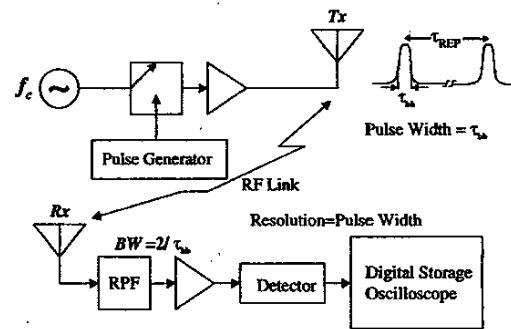


Figure 10a. A block diagram of the direct RF channel impulse-response measurement system.
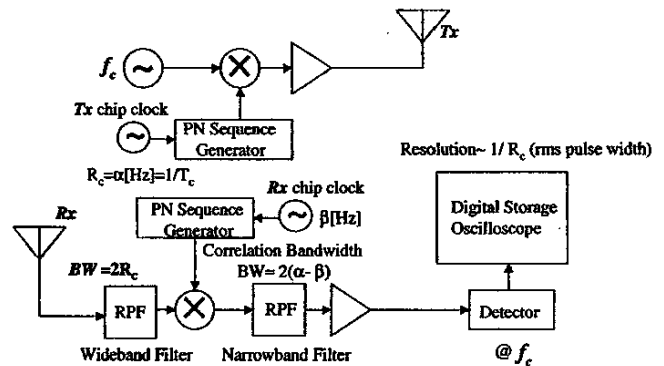


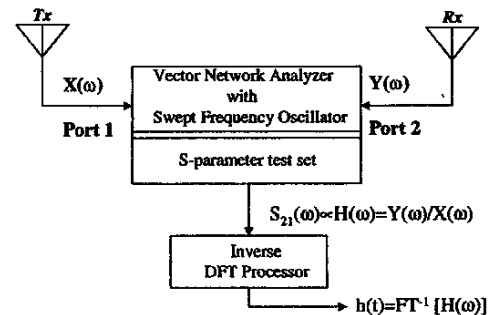Figure 10b. A block diagram of the spread-spectrum channel impulse measurement system.



Figure 10c. A block diagram of the frequency-domain channel impulse measurement.

**Table 5. Measurements and RMS delay spreads.**

| Technique | Location | $\tau_{RMS}$ (ns) | Frequency (MHz) | Ref. |
|---|---|---|---|---|
| B | Office building | 30-100 | 850, 1700 | [106] |
| A | Manufacturing floors | 15-29 (Area A)<br>31-62 (Area B)<br>48-90 (Area C)<br>52-57 (Area D)<br>19-37 (Area E) | 910 | [109] |
| A | Indoor sports arena<br>Open-plan factory<br>Textile plant<br>Office building | 7-120<br>40-130<br>15-125<br>5-40 | 1300<br>4000 | [110] |
| A | Within a room (4 rooms) | 7-16<br>10 ns (Med.) | 37200 | [111] |
| B | Urban area I<br><br>Urban area II | 98-1270<br>590 (Ave.)<br>61-2940<br>480 (Ave.) | 910 | [112] |
| C | Building 1<br>Building 2 | About 12-72<br>About 4-25 | 40000 | [113] |
| B | Sidewalk of LOS street | $0.5d + 40$<br>($d$ is T-R) | 2600 | [114] |
| A | Engineering bldg.<br>Retail store | 12.85-84.60<br>20.74-102.44 | 2400 | [115] |
| – | Laboratories at same floor | 8.3 LOS (Med.)<br>14.1 OLOS1 Med.<br>22.3 OLOS2 Med. | 910 | [117] |
| B | Outdoor Site 1<br>Site 2<br>Site 3 | 60-250, 130 (Med)<br>40-130, 70 (Med)<br>60-250, 120 (Med) | – | [118] |
| C | In two buildings | 10-50 with mean 20-30 | 900-1300 | [119] |
| C | Four types of indoor locations | 10-20 (Med )<br>10-20 (Med)<br>5-15 (Med) | 2400<br>4750<br>1150 | [108] |
| A | Hamburg<br>Dusseldorf<br>Frankfurt(bank)<br>Frankfurt(apart.) | 1300 (typical)<br>3100 (typical)<br>8100 (largest)<br>19600 (largest) | 942.225 | [120] |
| A | Washington<br>Greenbelt<br>Oakland<br>San Francisco | 2500-7500<br>2000-7000<br>2500-13500<br>1000-25500 | 892 | [121] |
| – | LOS (100-400 m) | 140.6-325.4 | 2197.5 | [122] |

**Table 6. The RMS delay spread as a function of the height of an antenna.**

| Antenna Height | Mean RMS Delay (ns) | Standard Deviation of RMS Delay (ns) | Location | Ref. |
|---|---|---|---|---|
| 3.7 m | 136.8 | 138.0 | San Francisco | [26] |
| 8.5 m | 176.8 | 147.1 | | |
| 13.3 m | 275.9 | 352.0 | | |
| 3.7 m | 134.6 | 127.4 | Ottawa | [123] |
| 8.5 m | 173.1 | 156.8 | | |

the height of the antenna. The predicted results can be bounded by an exponential model of the form $\tau_{RMS}(\text{ns}) = \exp(0.065 PL)$, where $PL$ is the path loss in decibels. Table 6 shows the measurements of $\tau_{RMS}$ with relation to the height of the antennas. It indicates that the delay spread increases as the antenna height increases, because as the antenna is raised, it becomes visible to more objects, scattering the electromagnetic radiation at greater distances.

## 6.2 Statistical Models of Time-Delay Spread

### 6.2.1 Two-Ray Rayleigh Fading Model

A commonly used multipath model is an independent Rayleigh fading two-ray model [10]. The impulse response of the model is represented by

$$h(t) = \alpha_1 \exp\left[j\theta_1(t)\right]\delta(t) + \alpha_2 \exp\left[j\theta_2(t)\right]\delta(t-\tau), \quad (39)$$

where $\alpha_1$ and $\alpha_2$ are independent random variables and have a Rayleigh PDF. $\theta_1$ and $\theta_2$ are also two independent random variables, and their density functions are uniformly distributed over $[0, 2\pi]$. $\tau$ is the time delay between the two rays.

### 6.2.2 Saleh and Valenzuela Model

Saleh and Valenzuela [30] reported the results of indoor measurements between two vertically polarized omnidirectional antennas, located on the same floor of a medium-sized office building. The measurements indicated that the statistics of the channel impulse response were independent of the polarizations of the transmitting and the receiving antennas if there was no line-of-sight path between them. The model assumed that the multipath components arrived in clusters. The clusters and components within a cluster formed a Poisson arrival process, with different rates.

### 6.2.3 Log-Normal at Any Distance

In [124], Cardoso and Mouliness presented three conjectures about delay spread. The first was that $\tau_{RMS}$ was log-normal at any distance. This was derived from measurement data that were classified into urban, suburban, rural, and mountainous areas. The second conjecture was that the median $\tau_{RMS}$ increased with distance, and the third conjecture was that $\tau_{RMS}$ tended to increase with shadow fading. $\tau_{RMS}$ can be given by

$$\tau_{RMS} = T_1 d^\varepsilon y, \quad (40)$$

where $T_1$ is the median value of $\tau_{RMS}$ at $d = 1\,\text{km}$, $\varepsilon$ is an exponent that lies between 0.5 and 1.0, and $y$ is the log-normal variable.

## 6.2.4 SIRCIM Model

Based on measurements at 1300 MHz in five factory and other types of buildings, the piecewise functions of excess delay for the probabilities of multipath arrivals were derived as [3]

$$P_R(T_K, S_1) = \begin{bmatrix} 1 - \dfrac{T_K}{367} & T_K < 110\,\text{ns} \\[2mm] 0.65 - \dfrac{(T_K - 110)}{360} & 110\,\text{ns} < T_K < 200\,\text{ns}, \\[2mm] 0.22 - \dfrac{(T_K - 200)}{1360} & 200\,\text{ns} < T_K < 500\,\text{ns} \end{bmatrix} \quad (41)$$

$$P_R(T_K, S_2) = \begin{bmatrix} 0.55 + \dfrac{T_K}{667} & T_K < 100\,\text{ns} \\[2mm] 0.08 + 0.62 e^{\frac{(T_K - 100)}{75}} & 100\,\text{ns} < T_K < 500\,\text{ns} \end{bmatrix} \quad (42)$$

where $S_1$ and $S_2$ correspond to LOS and obstructed LOS environments, respectively. $T_K$, in units of ns, is the excess delay at which a multipath component will arrive at the receiver, and takes on values that are integer multiples of 7.8 ns.

## 6.2.5 $\Delta - K$ Model

This model [9, 119] takes into account the clustering property of paths caused by the grouping property of scatters. The process is described by transitions between two states, representing different mean arrival rates. Initially, the process starts in State 1, with a mean arrival rate $\lambda_0(t)$. If a path arrives at time $t$, a transition is made to State 2, with a mean arrival rate $K\lambda_0(t)$. If no further paths arrive in the interval $[t, t+\Delta]$, a transition is made back to State 1 at the end of the interval.

## 6.2.6 Discrete-Time Model

In this model [119, 125], the time axis is divided into small time intervals, called "bins." Each bin is assumed to contain either one multipath component or no multipath component. The possibility of more than one path in a bin is excluded. A reasonable bin size is the resolution of the specific measurement.

## 6.3 Deterministic Models of Time-Delay Spread

The above statistical models are based on measurements made in a specific environment. They may not be suitable for prediction in other environments.

## 6.3.1 Ray Tracing

In theory, the ray-tracing technique [12, 105, 118, 123, 127] can determine almost all multipath components, including their amplitudes, time delays, and phases, and the technique is effective in predicting the time-delay spread. A detailed knowledge of the environment is required when applying a ray-tracing method. Another advantage of ray-tracing models over other propagation models are their ability to incorporate antenna radiation patterns and, in particular, to consider the effect of the radiation pattern individually on each ray.

Since the phase of each ray arriving at a receiver varies significantly with distance and cannot be accurately predicted, it will be impossible to achieve agreement with either the instantaneous measured shape or the value of the RMS delay spread for a single individual measurement. The comparison between measured and modeled results should be for average values in a small area around the actual mobile position [127]. A seven-ray and a 25-ray model consider only single or double reflections, respectively, and were used to simulate propagation in a room [105]. The RMS delay spread was predicted, and agreed well with that calculated from measurements.

## 6.3.2 VRP Model

This is similar to a seven-ray model, but in an outdoor environment. It assumed some virtual reflection points (VRPs), located at the intersection points along the LOS on streets and at building walls [122]. It did not consider the effects of traffic and moving humans. The predicted results for the RMS delay spreads were verified by measurements.

## 7. Joint Angle-Delay Estimation (JADE)

In mobile communications systems, the multipath channel is characterized not only by the various time delays of the different propagation paths, but also by their directions of arrival (DOA) or angles of arrival (AOA). Estimating the time delay by ignoring the spatial characteristics of the multipath channel – as most systems now do – is definitely not optimum. Indeed, exploiting the spatial structure by using adaptive antenna systems and properly estimating the delays can improve the characterization of the channel and, consequently, can lead to better system service.

The joint angle- and delay-estimation technique is, in fact, often employed in radars using space-time concepts. In comparison to disjoint techniques – which first estimate delays and, subsequently, the angle corresponding to each delay – joint estimation has a number of advantages. First, the relative delay estimates between two or more synchronized base stations can be used, in conjunction with the DOA information, to estimate the location of the mobile unit. Second, it is theoretically possible to exploit the difference in path delays to improve angle-estimation accuracy, and vice-versa [8, 152]. Third, when several angles are detected, the most-probable portable direction is the one that is associated with the smallest delay, because the direct path has the shortest propagation time. Unfortunately, the problem with this model – even though the formulation is quite esoteric from a signal-processing point of view – is that the directions of arrival and the time delays of the signals are not independent quantities. The two

parameters are intimately related through the distance between the source and the field point, and the velocity of light. Hence, a basic physical understanding of the problem is absolutely essential in trying to obtain a meaningful solution. There are several variations of this technique, which is often abbreviated as JADE.

## 7.1 JADE Maximum-Likelihood Model [8, 153]

In the conditional-maximum method, the vector representing the complex envelope of the fading path is assumed to be non-random. Under this assumption, the maximum-likelihood-method estimates of the angle of arrival and the time delay are obtained by minimizing the cost function. In the unconditional-maximum method, the envelope of the fading path is assumed to be a stationary Gaussian random process, and a different cost function is obtained. It involves a $2L$-dimensional optimization over both the angles of arrivals and the time delays, where $L$ is the number of multipath components. Hence, it is computationally prohibitive, even for moderate values of $L$. In [153], an efficient method in which $\theta$ and $\tau$ were estimated in parallel was developed.

## 7.2 JADE-MUSIC Model [154]

A faster – though suboptimal – approach is based on the MUSIC algorithm, and involves only a two-dimensional search. The MUSIC method estimates the angles of arrival and the delay parameters by finding the $L$ minima of the pseudo-spectrum.

## 7.3 SI-JADE Model [155,156]

By assuming a uniform time sampling and a uniform linear array, this algorithm transforms the data using a discrete Fourier transform (DFT), and performs a deconvolution with the known pulse-shape function. It then stacks the result into a Hankel matrix. This reduces the problem to one that can be solved using a two-dimensional ESPRIT algorithm. The algorithm can thus be written in closed form and is computationally attractive.

## 7.4 JADE-ESPRIT Model [157]

If the array is a uniform linear antenna array, or if it has the ESPRIT doublet-structure, then the angles and delays can be estimated jointly. The JADE-ESPRIT algorithm requires stricter identifiably conditions, and can deal with the number of resolvable paths that are determined by the number of samples available. This model is quite similar to the SI-JADE algorithm. SI-JADE, however, only acts on a single-channel estimate, and may also introduce an undesired coupling between angle and delay estimates in the case where the model is not perfectly valid.

There are other techniques in addition to the JADE models, such as the subspace-based methods [158], and a Bayesian-based model [159]. The Cramer-Rao bound (CRB) has been derived for each of these models. However, only simulation results have been used to verify all these models.

To conclude this section, it is important to point out that all these models treat each antenna as an isotropic radiator. An admirer of James Clark Maxwell will immediately realize that such an antenna does not exist in the electromagnetics world, which is the domain of wireless, but does exist in the acoustic arena. The smallest antenna is a Hertzian dipole, and even that has a directional pattern; however, it may be omnidirectional in certain planes. Finally, we point out that an electrically small antenna differentiates the pulse on transmission, and integrates or samples the signal on reception. However, for finite-length antennas, the radiated fields are proportional to the double derivative of the current induced on the structure. On reception, the open-circuit voltages are proportional to the single derivative of the incident fields. Hence, unless the impulse responses of the transmitting and receiving antennas are included in a broadband channel characterization, it is difficult to see how one can obtain a meaningful physical model of the wireless propagation channel!

# 8. Epilogue

However, in a mobile communication environment where there is an established two-way communication, it is not necessary to know these path propagation models in order to direct the energy from the transmitter to a pre-specified mobile. It is not even necessary to know the particular electromagnetic environment in which they are transmitting. It is not even necessary to have any knowledge about the spatial locations of the transmitters and the receivers. This can be accomplished using the principle of reciprocity. The details are available in [160]. A brief description of this novel technique is provided here.

In this novel procedure, we simultaneously employ the concept of reciprocity and use the principle of adaptivity on transmission. In this way, it is possible to direct the energy transmitted from a base station to a pre-selected mobile station, without worrying about either the presence of other near-field scatterers or the existence of a multipath environment. For example, consider the system represented in Figure 11. Here, let us assume, for example, that the transmitter is sending signals using spatial diversity, i.e., using a number of transmitting antennas spatially separated from each other. Let us assume that transmitting antenna #1 is transmitting a voltage $V_{T_1}$ at a frequency $f_0$. The internal impedance of this voltage source is $R_{T_1}$. At the second transmitting antenna, we have a voltage source $V_{T_2}$ transmitting at the same frequency, with an internal impedance of $R_{T_2}$. In addition, there are two receivers, represented by $R_1$ and $R_2$. The goal of this transmitting system is that we want to maximize the received power at receiver 1 by exciting transmitting systems 1 and 2 with voltages $V_{T_1}^1$ and $V_{T_2}^1$. Our goal is to minimize the received power at receiver 2 while directing the energy to receiver 1. Similarly, we want to find another set of voltages, $V_{T_1}^2$ and $V_{T_2}^2$, that will excite the two trans-
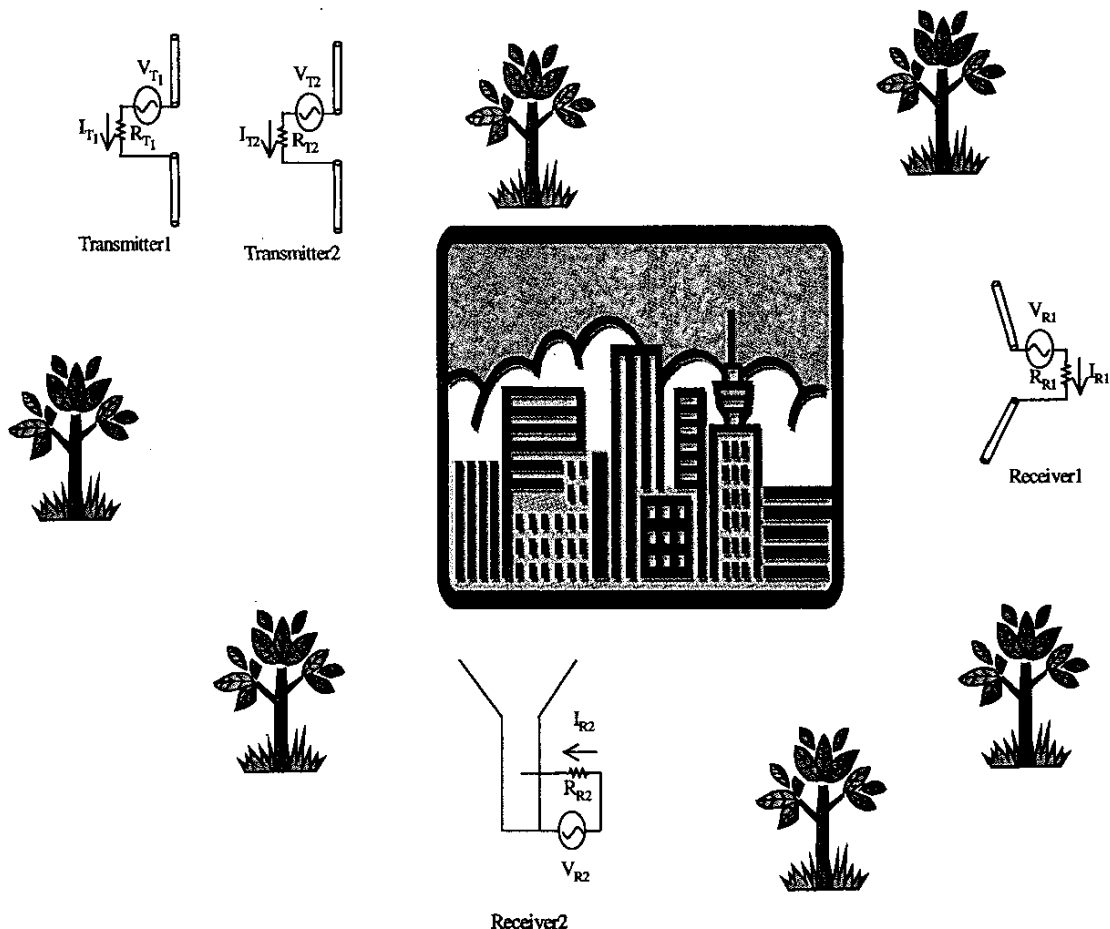


**Figure 11. A multiple-user transmit/receive scenario.**

mitting antennas so that they will induce zero fields on receiver #1 (designated by $R_1$) and maximum fields at receiver #2 (designated by $R_2$). The characteristics of these two voltage sets with a superscript of 2 are such that when they are used to excite the transmitting antennas, the electromagnetic signal will be directed to receiver 2 and will induce practically no energy at receiver 1. In this way, we can essentially do adaptivity on transmission. This is ideally suited in a CDMA (code-division multiple access) environment, for example, where a unique code is assigned to each receiver, so that when we receive any signal we know from which receiver it originated. When we are going to transmit that particularly weighted signal, broadcast simultaneously over all the transmitting antennas, we can spatially direct the energy to a pre-specified receiver only, and simultaneously minimize the received signals at the other receivers for which that particular transmission was not intended. In this way, it is possible to direct the energy to a pre-selected receiver.

The problem now is, how to carry this out? We propose to achieve this objective using the principle of reciprocity. Reciprocity tells us that if we excite transmitting antenna #1 with a voltage $V_{T_1}$ and with the other voltages set to zero, such that $V_{T_2} = V_{R_1} = V_{R_2} = 0$, then the transmitted signal will induce a current, $I_{R_1}$, at the feed point of the receiving antenna marked #1 (i.e., $R_1$). It will also induce currents at receiver #2 and transmitter #2. However, let us ignore that for the moment. Under the same environment, if we excite receiver 1 with a voltage $V_{R_1}$ with $V_{T_1} = V_{T_2} = V_{R_2} = 0$, then it will induce a current – let us say, $I_{T_1}$ – at transmitter #1. It will also induce currents at receiver #2 and transmitter #2. However, let us also ignore these for the moment. Then, from the principle of reciprocity, we know that

$$V_{T_1} I_{T_1} = V_{R_1} I_{R_1}. \tag{43}$$

Equation (43) represents the reciprocity theorem in the frequency domain. The relationship is much more involved in the time domain, where the reciprocity theorem performs an integration over time. That is why it is possible – without violating the principle of reciprocity – for a transmitting antenna to radiate essentially a differentiated version of the temporal input waveform applied to it, whereas a receiving antenna integrates the incident signal, both spatially and in the temporal domain.

Here, we consider the currents that are induced at the transmitting and receiving antennas to be at the loads that are associated with the feed point of each antenna. The relationship provided by Equation (43) is valid irrespective of the shape of the transmitting or receiving antennas. It also does not depend on the presence of various near-field scatterers, like trees or buildings that are in the immediate neighborhood of the transmitting or the receiving antennas, as illustrated in Figure 11. One does not even require any knowledge about the spatial locations of the various antennas. The principle of reciprocity can help one to treat such a complex situation without any knowledge of either the electromagnetic environment in which the antennas are communicating, and it is not necessary to know the spatial locations of objects that influence the electromagnetic coupling mechanisms. Based on the principle of reciprocity, we now implement the system of adaptivity on transmission.

Let us assume that each receiver is given a particular code, as in a CDMA environment. Let us assume that we transmit the code with amplitude 1 V. So, when $V_{R_1} = 1$ V with $V_{R_2} = V_{T_1} = V_{T_2} = 0$,

then it is going to induce currents $I_{T_1}^1$ in transmitting antenna #1, and $I_{T_2}^1$ in transmitting antenna #2. From these induced currents, we know the voltage induced across the loads of the transmitting antennas, since we know the impedance values of the loads. Now, what the reciprocity principle tells us is that if we apply 1 V at the feed of the transmitting antenna #1, so that $V_{T_1} = 1$ and $V_{T_2} = V_{R_1} = V_{R_2} = 0$, then it will induce a current $I_{R_1}^1$ into receiver 1, so that

$$I_{T_1}^1 = I_{R_1}^1. \tag{44}$$

Similarly, if we excite receiver 2 only with a voltage of 1 V, so that $V_{R_2} = 1$ V and $V_{T_1} = V_{T_2} = V_{R_1} = 0$, then this will induce currents $I_{T_1}^2$ and $I_{T_2}^2$ at transmitters 1 and 2, respectively. From reciprocity, we have the result that if we excite transmitter 2 with 1 V at the same frequency $f_0$, then $V_{T_2} = 1$ and $V_{T_1} = V_{R_1} = V_{R_2} = 0$. Under this situation, there will be an induced current $I_{R_2}^2$ in receiver 2. From the principles of reciprocity in the frequency domain, one obtains

$$I_{T_2}^2 = I_{R_2}^2. \tag{45}$$

It is important to observe that reciprocity only links the two transmitting and receiving ports under consideration, namely, those related to the transmitter and the receiver. The other portions of the electromagnetic network do not come into the picture, as long as it remains the same when we switch the voltages on the transmitters and receivers to satisfy the relationships of Equations (44) and (45). Nor is reciprocity dictated by the material medium influencing the propagation path. This implies that the propagation that resulted in the induced currents described by the variables in Equations (44) and (45) can occur even when one is communicating in non-isotropic and heterogeneous media.

From the above observations, we can carry out the following procedure:

**Step 1:** Excite receiver #1 with 1 V, with $V_{T_1} = V_{T_2} = V_{R_2} = 0$. This will induce currents $I_{T_1}^1$ and $I_{T_2}^1$ in transmitting antennas 1 and 2, respectively. Let us assume that we can measure these currents.

**Step 2:** Excite receiver #2 with 1 V, with $V_{T_1} = V_{T_2} = V_{R_1} = 0$. This will induce currents $I_{T_1}^2$ and $I_{T_2}^2$ in transmitting antennas 1 and 2, respectively. Let us assume that we can measure these two currents. The measurement is easy to carry out in a CDMA environment, where each receiver carries a unique code.

**Step 3:** If we now excite transmitter 1 with a voltage $W_1^1$ and transmitter 2 with a voltage $W_2^1$, then the current induced in receiver 1 will be the sum of the following two terms: $W_1^1 I_{T_1}^1 + W_2^1 I_{T_2}^1$. Of course, this is under the assumption that all the loads terminating the two transmitting and the receiving antennas are all equal and numerically equal to $R_{T_1} = R_{T_2} = R_{R_1} = R_{T_2} = 1\,\Omega$. The induced current at receiver 2 under these conditions will be $W_1^1 I_{T_1}^2 + W_2^1 I_{T_2}^2$. If the signal is to be

directed to receiver 1 and not to receiver 2, then the weights $W_1^1$ and $W_2^1$ should be such that the first sum should be unity and the second sum should be zero. Equivalently, if we now excite transmitter 1 with a voltage $W_1^2$ and transmitter 2 with a voltage $W_2^2$, then the current induced in receiver 1 will be the sum of these two terms: $W_1^2 I_{T_1}^1 + W_2^2 I_{T_2}^1$. In receiver 2, the induced current will be $W_1^2 I_{T_1}^2 + W_2^2 I_{T_2}^2$. If we were to direct the signal to receiver 2 and not to receiver 1, then, the first sum should be zero and the second sum should be unity. Therefore, by appropriate choice of the voltages exciting the two transmitting antennas, it is possible to direct the signal to a receiver chosen a priori, irrespective of the near-field electromagnetic environment in which they may be operating. In summary, the four equations described above that can direct the transmitted energy to a pre-selected receiver can be written in a compact matrix form as

$$\begin{bmatrix} I_{T_1}^1 & I_{T_2}^1 \\ I_{T_1}^2 & I_{T_2}^2 \end{bmatrix} \begin{bmatrix} W_1^1 & W_1^2 \\ W_2^1 & W_2^2 \end{bmatrix} = \begin{bmatrix} 1 & 0 \\ 0 & 1 \end{bmatrix}. \tag{46}$$

No loss of generality will occur with the choice of a value different that $1\,\Omega$ for the impedance terminating both the transmitting and the receiving antennas, since it will only affect the scale factor for all four of the weights.

**Step 4:** Solution of Equation (46) provides the set of weights that, when used in conjunction with the signals received from the two receivers producing currents at the transmitters, will direct the transmitted energy to receiver 1 or to receiver 2, depending on the values of the weights chosen. Hence,

$$\begin{bmatrix} W_1^1 & W_1^2 \\ W_2^1 & W_2^2 \end{bmatrix} = \begin{bmatrix} I_{T_1}^1 & I_{T_2}^1 \\ I_{T_1}^2 & I_{T_2}^2 \end{bmatrix}^{-1} \begin{bmatrix} 1 & 0 \\ 0 & 1 \end{bmatrix}. \tag{47}$$

The caveat here is that if we apply a voltage equal to $W_1^1$ on transmitting antenna #1 and $W_2^1$ on transmitting antenna #2 then the electromagnetic energy received from these two transmitting antennas will add vectorially at the terminals of receiver #1, and will be destructive at the terminals of receiver #2, producing zero current at its loads. In contrast, if we apply the voltages $W_1^2$ on transmitting antenna #1 and $W_2^2$ on transmitting antenna #2, then the received electromagnetic energy will be vectorially destructive at the terminals of receiver #1, resulting in practically zero current flowing through its load, and will add vectorially at the terminals of receiver #2, producing a large value for the induced current.

In summary, by knowing the voltages that are induced at each of the transmitting antennas due to each one of the receivers, it is possible to select a set of weights based on reciprocity. This relationship, based on reciprocity, can be applied only at the terminals of the transmitting and receiving antennas. It is independent of the size and shapes of the receiving antennas, nor does it depend on the near-field environment.

Now, if there are more receivers than transmitting antennas, then it may not be possible to achieve a perfect match (namely, simultaneously directing the received energy to a pre-selected receiver and having practically zero energy induced on the rest of the receivers), but some intermediate solution will still be possible. We now illustrate these statements through examples.

## 8.1 Numerical Simulations

As an example, consider three transmitting antennas, $A_1$, $A_2$, and $A_3$, located at a base station. The three antennas are considered to be three dipoles of radius 5 mm, and their lengths are 15 cm. If the operating frequency is 1 GHz, the three antennas are a half-wavelength long. Next, we consider three receiving antennas, marked as $A_4$, $A_5$, and $A_6$, as shown in Figure 12. They are spaced with a half wavelength between themselves, and they are separated from the transmitters by a distance of 2 m. In this simulation, we want to demonstrate that by choosing a proper set of weighted excitations on the transmitters $A_1$, $A_2$, and $A_3$ it is possible to direct the electromagnetic energy in such a way that it will add vectorially at only one receiver (say, $A_4$), and that the voltages received from these three transmitting antennas will combine vectorially in such a way that they will produce practically zero currents at the terminals of the remaining two receivers, $A_5$ and $A_6$. In a similar fashion, it is possible to select another set of weights that will result in receiver $A_5$ developing a large signal at its terminals, while the signals received at the terminals of the other two receivers, $A_4$ and $A_6$, will be practically zero, and so on.

We now illustrate how this can be accomplished based on the principles of reciprocity. First, we excite receiver 1 with 1 V, and that will induce a current in both receivers $A_5$ and $A_6$, and also in transmitters $A_1$, $A_2$, and $A_3$, comprising the base station. These induced currents will generate voltages across the loads of the remaining five centrally loaded dipole antennas. Let us call the voltages received at transmitters $A_1$, $A_2$, and $A_3$, due to an excitation voltage of 1 V at receiver $A_4$, $V_{A_1}^1$, $V_{A_2}^1$, and $V_{A_3}^1$, respectively. Similarly, if we excite the antenna at the mobile, $A_5$, with 1 V, then the voltages received at the three base-station antennas will be $V_{A_1}^2$, $V_{A_2}^2$, and $V_{A_3}^2$. Even though voltages are also induced in the other two receivers, they are of no consequence. Finally, if we excite receiver $A_6$ with 1 V, then it will generate the following voltages at the three transmitters: $V_{A_1}^3$, $V_{A_2}^3$, and $V_{A_3}^3$. Now, the claim is that, based on the available information from the above three experiments, we can choose a set of complex
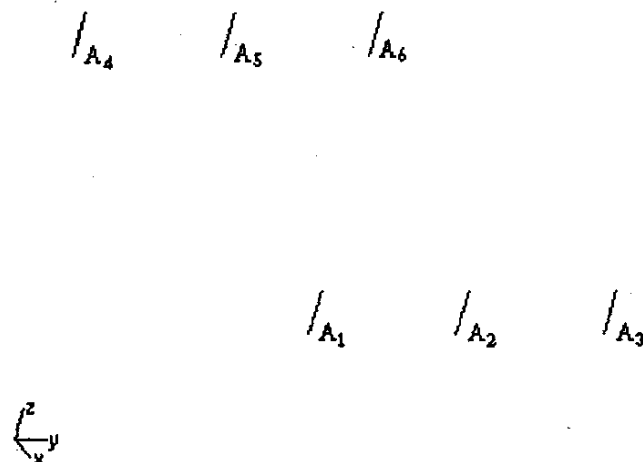
$/_{A_4}$  $/_{A_5}$  $/_{A_6}$

$/_{A_1}$  $/_{A_2}$  $/_{A_3}$

**Figure 12. A six-antenna system.**

voltages $W_1^1$, $W_2^1$, and $W_3^1$ that, when fed to the three transmitting antennas, will result in an vectorial additive combination of the electromagnetic energy at receiver 1, while simultaneously inducing practically no currents in the other two receivers. From the principle of reciprocity, we are going to evaluate the induced currents at the loads located at the feed points of the three receivers, when all of the three transmitting antennas $A_1$, $A_2$, and $A_3$ are simultaneously excited with the voltages $W_1^1$, $W_2^1$, and $W_3^1$. The receiver currents at the three locations will then be

At Receiver 1: $W_1^1 I_{A_1}^1 + W_2^1 I_{A_2}^1 + W_3^1 I_{A_3}^1$

At Receiver 2: $W_1^1 I_{A_1}^2 + W_2^1 I_{A_2}^2 + W_3^1 I_{A_3}^2$

At Receiver 3: $W_1^1 I_{A_1}^3 + W_2^1 I_{A_2}^3 + W_3^1 I_{A_3}^3$

The objective is now to select the weights $W$ in such a fashion that the voltage received will be finite at receiver 1, and zero at receivers 2 and 3. This is enforced through the following equation:

$$\begin{bmatrix} I_{A_1}^1 & I_{A_2}^1 & I_{A_3}^1 \\ I_{A_1}^2 & I_{A_2}^2 & I_{A_3}^2 \\ I_{A_1}^3 & I_{A_2}^3 & I_{A_3}^3 \end{bmatrix} \begin{bmatrix} W_1^1 \\ W_2^1 \\ W_3^1 \end{bmatrix} = \begin{bmatrix} 1 \\ 0 \\ 0 \end{bmatrix}. \tag{48}$$

Now, if the three transmitting antennas are excited with the following three complex voltages, obtained from the solution of Equation (48),

$W_1^1 = -0.415 + j0.366$,

$W_2^1 = -0.679 - j0.446$,

$W_3^1 = 0.845 + j0.062$,

then the electromagnetic energy will add vectorially at the terminals of receiver 1, and the received voltages will cancel each other resulting in practically zero currents at the terminals of the other two receivers. Based on these three voltages, we carried out an electromagnetic simulation using *WIPL-D* [161], and obtained the following three induced currents in the three receivers (with $R_{T_1} = R_{T_2} = R_{T_3} = 50\,\Omega$):

$I_{T_1} = 1.0 - j0.007$,

$I_{T_2} = -0.003 + j0.001$,

$I_{T_3} = 0.001 - j0.002$

(all the currents are in mA).

This clearly shows that for this particular choice of the excitation voltages, the electromagnetic environment will be such that it will induce a large current at the load of receiver 1, and practically zero currents at the terminals of the other two receivers. This in no way implies that the current distribution on the receiving antenna is zero. It is not. It is practically zero only at the feed terminals and nowhere else! This is because the principle of reciprocity only holds at the pre-specified terminals or ports of a network.

Similarly, using the above procedure, one can show that if the excitation voltages are chosen for the three transmitting antennas as follows:

$W_1^2 = -0.679 - j0.446$,

$W_2^2 = 0.137 + j0.011$,

$W_3^2 = -0.679 - j0.446$,

then the currents induced at the terminals of the three receivers will be given by

$I_{T_1} = -0.003 - j0.0003$,

$I_{T_2} = 1.0 - j0.01$,

$I_{T_3} = -0.003 + j0.0003$

(all the currents are in mA),

which clearly shows that the induced energy can be vectorially additive at only receiver 2, while producing no appreciable currents at the terminals of the other two receivers, 1 and 3.

Finally, if the excitation voltages at the three transmitting antennas are chosen to be

$W_1^3 = 0.845 + j0.062$,

$W_2^3 = -0.679 - j0.446$,

$W_3^3 = -0.415 + j0.366$,

then one can show that the currents induced at the terminals of the three receivers will be

$I_{T_1} = -0.0012 - j0.0025$,

$I_{T_2} = -0.003 + j0.001$,

$I_{T_3} = 1.0 - j0.007$

(all the currents are in mA).

This clearly demonstrates that by appropriately choosing the three complex amplitudes of the excitations at different transmitting antennas simultaneously it is possible to create an electromagnetic environment such that the induced electromagnetic energy will be vectorially additive at any one of the terminals of the pre-selected receivers, and that the received voltages will try to cancel each other at the terminals of the other receiving antennas, resulting in practically zero current. Such a procedure can be carried out without knowing precisely the near-field environment in which the transmitter and the receiver are operating, and without knowing the precise spatial locations of the transmitting or the receiving antennas.

In summary, the steps involved in this new method are as follows:

**Step 1:** Excite each of the mobile receiving antennas and measure the currents that are induced in the base-station transmitting antennas.

**Step 2:** Using these induced currents, generate a matrix, the inversion of which will contain the information necessary to excite the transmitting antennas.

**Step 3:** Then, depending on the choice of which of the mobile receiving antennas the signal is meant for, a set of weights can be solved for that will result in a vectorial addition of all the incident electromagnetic energy at the terminals, maximizing the induced currents. This will produce the maximum voltage at that pre-determined receiver, and practically zero induced currents at the terminals of the other receivers.

By following the above procedure, one can carry out adaptivity on transmission based on the principle of reciprocity. This methodology works even when there are near-field scatterers. From our numerical simulations [160], we observed that this principle can be applied over a relatively wide band of frequencies. Hence, when the ports of a communication system are well defined, the propagation-path modeling can be avoided through the use of the principle of reciprocity, at least in this case.

# 9. Conclusions

Propagation models are needed not only for installation guidelines, but they also play a key part in any analysis or design that strives to mitigate interference. In this paper, we have surveyed some of the typical propagation models that provide good estimates for both large-scale and small-scale fading channels. Despite the enormous efforts to date, much work remains in understanding and predicting the characteristics of mobile communications channels. In addition, an efficient ray-tracing method has been presented for tracing rays in an indoor propagation system. An FDTD method has been described to analyze wave propagation through the walls in a building. Finally, it has been seen that the principle of reciprocity can be applied to direct the transmitted energy to a pre-specified mobile unit without having any a priori knowledge of the electromagnetic environment.

# 10. Acknowledgement

# 11. References

1. H. L. Bertoni, *Radio Propagation for Modern Wireless Systems*, Upper Saddle River, NJ, Prentice Hall PTR, 2000, pp. 90-92.

2. J. B. Andersen, T. S. Rappaport, and S. Youshida, "Propagation Measurement and Models for Wireless Communications Channels," *IEEE Communications Magazine*, 33, 1, January 1995, pp. 42-49.

3. T. S. Rappaport, S. Y. Seidel, and K. Takamizawa, "Statistical Channel Impulse Response Models for Factory and Open Plan Building Radio Communicate System Design," *IEEE Transactions on Communications*, COM-39, 5, May 1991, pp. 794-807.

4. W. C. Y. Lee, *Mobile Cellular Telecommunications Systems*, New York, McGraw Hill Publications, 1989.

5. B. Sklar, "Rayleigh Fading Channels in Mobile Digital Communication Systems. Part I," *IEEE Communications Magazine*, 35, 9, 1997, pp. 136-146.

6. L. C. Godara, "Applications of Antenna Arrays to Mobile Communications. Part I. Performance Improvement, Feasibility, and System Considerations," *Proceedings of the IEEE*, 85, 7, July 1997, pp. 1031-1060.

7. M. Chryssomallis, "Smart Antennas," *IEEE Antennas and Propagation Magazine*, 42, 3, June 2000, pp. 129-136.

8. G. G. Raleigh and T. Boros, "Joint Space-Time Parameter Estimation for Wireless Communication Channels," *IEEE Transactions on Signal Processing*, 46, 5, May 1998, pp. 1333-1343.

9. G. L. Turin, "A Statistical Model for Urban Multipath Propagation," *IEEE Transactions on Vehicular Technology*, VT-21, 1, 1972, pp. 1-9.

10. T. S. Rappaport, *Wireless Communications: Principles & Practice*, Upper Saddle River, NJ, Prentice Hall PTR, 1996.

11. M. F. Catedra, J. Perez, F. Saez de Adana, and O. Gutieerez, "Efficient Ray-Tracing Techniques for Three Dimensional Analyses of Propagation in Mobile Communications: Application to Picocell and Microcell Scenarios," *IEEE Antennas and Propagation Magazine*, 40, 2, April 1998, pp. 15-27.

12. S. Y. Seidel and T. S. Rappaport, "Site-Specific Propagation Prediction for Wireless In-Building Personal Communication System Design," *IEEE Transactions on Vehicular Technology*, VT-43, 4, 1994, pp. 879-891.

13. D. Molkdar, "Review on Radio Propagation into and within Buildings," *IEE Proceedings-H*, 138, 1, Feb. 1991, pp. 61-73.

14. T. Okumura, E. Ohmori, and K. Fukuda, "Field Strength and its Variability in VHF and UHF Land Mobile Service," *Review Electrical Communication Laboratory*, 16, 9-10, 1968, pp. 825-873.

15. M. Hata, "Empirical Formula for Propagation Loss in Land Mobile Radio Service," *IEEE Transactions on Vehicular Technology*, VT-29, 3, 1980, pp. 317-325.

16. J. Walfisch and H. L. Bertoni, "A Theoretical Model of UHF Propagation in Urban Environments," *IEEE Transactions on Antennas and Propagation*, AP-36, 12, 1988, pp. 1788-1796.

17. K. Low, "Comparison of Urban Propagation Models with CW-Measurements," *IEEE Vehicular Technology Society 42nd VTS Conference. Frontiers of Technology. From Pioneers to the 21st Century*, 2, 1992, pp. 936-942.

18. S. R. Saunders and F. R. Bonar, "Explicit Multiple Building Diffraction Attenuation Function for Mobile Radio Wave Propagation," *Electronics Letters*, 27, 14, July 1991, pp. 1276-1277.

19. S. R. Saunders and F. R. Bonar, "Prediction of Mobile Radio Wave Propagation over Buildings of Irregular Heights and Spac-

ings," *IEEE Transactions on Antennas and Propagation*, **AP-42**, 2, 1994, pp. 137-144.

20. M. J. Neve and G. B. Rowe, "Assessment of GTD for Mobile Radio Propagation Prediction," *Electronics Letters*, **29**, 7, April 1993, pp. 618-620.

21. L. Juan-Llacer and N. Cardona, "UTD Solution for the Multiple Building Diffraction Attenuation Function for Mobile Radiowave Propagation," *Electronics Letters*, **33**, 1, April 1997, pp. 92-93.

22. L. Juan-Llacer, L. Ramos, and N. Cardona, "Application of Some Theoretical Models for Coverage Prediction in Macrocell Urban Environments," *IEEE Transactions on Vehicular Technology*, **VT-48**, 5, 1999, pp. 1463-1468.

23. D. Har, A. M. Watson, and A. G. Chadney, "Comment on Diffraction Loss of Rooftop-to-Street in Cost 231-Walfich-Ikegami Model," *IEEE Transactions on Vehicular Technology*, **VT-48**, 5, 1999, pp. 1451-1452.

24. T. S. Rappaport and L. B. Milstein, "Effect of Radio Propagation Path Loss on DS-CDMA Cellular Frequency Reuse Efficiency for the Reverse Channel," *IEEE Transactions on Vehicular Technology*, **VT-41**, 3, August 1992, pp. 231-242.

25. H. Xia, H. L. Bertoni, L. R Maciel, A. Lindsay-Stewart, and R. Rowe, "Radio Propagation Characteristics for Line-of-sight Microcellular and Personal Communications," *IEEE Transactions on Antennas and Propagation*, **AP-41**, 10, October 1993, pp. 1439-1447.

26. M. J. Feuerstein, K. L Blackard, T. S. Rappaport, S. Y. Seidel, and H. H. Xia, "Path Loss, Delay Spread, and Outage Models as Functions of Antenna Height for Macrocellular System Design," *IEEE Transactions on Vehicular Technology*, **VT-43**, 3, August 1994, pp. 487-498.

27. N. Beaunstein, "Prediction of Cellular Characteristics for Various Urban Environments," *IEEE Antennas and Propagation Magazine*, **41**, 6, 1999, pp. 135-145.

28. S. Ichitsubo, T. Furuno, T. Taga, and R. Kawasaki, "Multipath Propagation Model for Line-of-Sight Street Microcells in Urban Area," *IEEE Transactions on Vehicular Technology*, **VT-49**, 2, 2000, pp. 422-427.

29. T. S. Rappaport and S. Sandhu, "Radio-Wave Propagation for Emerging Wireless Personal-Communication Systems," *IEEE Antennas and Propagation Magazine*, **36**, 5, October 1994, pp. 14-24.

30. A. A. M. Saleh and R. L. Valenzuela, "A Statistical Model for Indoor Multipath Propagation," *IEEE Journal on Selected Areas in Communications*, **5**, 2, 1987, pp. 128-137.

31. R. J. C. Bultitude, "Measurement Characterization and Modeling of Indoor 800/900 MHz Radio Channels for Digital Communications," *IEEE Communications Magazine*, **5**, 6, 1987, pp. 5-12.

32. F. C. Owen and C. D. Pundey, "In-Building Propagation at 900 MHz and 1650 MHz for Digital Cordless Telephone," 6th Int. Conf. on Antennas and Propagation, ICAP'89, Part 2: Propagation, 1989, pp. 276-281.

33. P. Valch, B. Segal, J. Lebel, and T. Pavlasek, "Cross-Floor Signal Propagation Inside a Contemporary Ferro-Concrete Building at 434, 864, and 1705 MHz," *IEEE Transactions on Antennas and Propagation*, **AP-47**, 7, 1999, pp. 1230-1232.

34. S. E. Alexander, "Characterising Buildings for Propagation at 900 MHz," *Electronics Letters*, **19**, 20, September 1983, p. 860.

35. S. Y. Seidel and T. S. Rappaport, "914 MHz Path Loss Prediction Models for Indoor Wireless Communications in Multifloored Buildings," *IEEE Transactions on Antennas and Propagation*, **AP-40**, 1992, pp. 207-217.

36. T. S. Rappaport, "Characterization of UHF Multipath Radio Channels in Factory Buildings," *IEEE Transactions on Antennas and Propagation*, **AP-37**, 8, August 1989, pp. 1058-1069.

37. K. Pahlavan, R. Ganesh, and T. Hotaling, "Multipath Propagation Measurements on Manufacturing Floors at 910 MHz," *Electronics Letters*, **25**, 3, February 1989, pp. 225-227.

38. D. A. Haand, "Indoor Wide Band Radio Wave Propagation and Models at 1.3 GHz and 4.0 GHz," *Electronics Letters*, **26**, 21, October 1990, pp. 1800-1802.

39. Telesis Technologies Laboratory, *"Experimental License Report to FCC,"* August 1991.

40. D. M. J. Davasirvatham, "A Comparison of Time Delay Spread and Signal Level Measurements within Two Dissimilar Office Buildings," *IEEE Transactions on Antennas and Propagation*, **AP-35**, 3, March 1987, pp. 319-324.

41. K. W. Cheung, J. H. M. Sau, and R. D. Murch, "A New Empirical Model for Indoor Propagation Prediction," *IEEE Transactions on Vehicular Technology*, **VT-47**, 3, August 1998, pp. 996-1001.

42. W. Honcharenko, H. L. Bertoni, and J. Dailing, "Mechanisms Governing UHF Propagation on Single Floors in Modern Office Buildings," *IEEE Transactions on Antennas and Propagation*, **AP-41**, 4, 1992, pp. 496-504.

43. S. Ruiz, Y. Samper, J. Perez, R. Agusti, and J. Olmos, "Software Tool for Optimising Indoor/Outdoor Coverage in a Construction Site," *Electronics Letters*, **34**, 22, October 1998, pp. 2100-2101.

44. G. M. Whitman, K. S. Kim, and E. Niver, "A Theoretical Model for Radio Signal Attenuation Inside Buildings," *IEEE Transactions on Vehicular Technology*, **VT-44**, 3, August 1995, pp. 621-629.

45. R. J. Luebbers, "Finite Conductivity Uniform GTD versus Knife Edge Diffraction in Prediction of Propagation Path Loss," *IEEE Transactions on Antennas and Propagation*, **AP-32**, 1, January 1984, pp. 70-76.

46. F. Ikegami, T. Takeuchi, and S. Yoshida, "Theoretical Prediction of Mean Field Strength for Urban Mobile Radio," *IEEE Transactions on Antennas and Propagation*, **AP-39**, 3, March 1991, pp. 299-302.

47. W. K. Tam and V. N. Tran, "Propagation Modeling for Indoor Wireless Communication," *Electronics & Communication Engineering Journal*, October 1995, pp. 221-228.

48. J. W. Mckown and R. L. Hamilton, Jr., "Ray Tracing as a Design Tool for Radio Networks," *IEEE Network Magazine*, **5**, Nov. 1991, pp. 27-30.

49. S. Y. Tan and H. S. Tan, "Improved Three-Dimension Ray Tracing Technique for Microcellular Propagation," *Electronics Letters*, **31**, 17, August 1995, pp. 1503-1505.

50. S. Y. Tan and H. S. Tan, "Propagation Model for Microcellular Communications Applied to Path Loss Measurements in Ottawa City Streets," *IEEE Transactions on Vehicular Technology*, **VT-44**, 2, May 1995, pp. 313-317.

51. S.Y. Tan and H.S. Tan, "A Theory for Propagation Path-Loss Characteristics in a City-Street Grid," *IEEE Transactions on Electromagnetic Compatibility*, **EMC-37**, 3, August 1995, pp. 333-342.

52. M. G. Sanchez, L. de Haro, A. G. Pino, and M. Calvo, "Exhaustive Ray Tracing Algorithm for Microcellular Propagation Prediction Models," *Electronics Letters*, **32**, 7, March 1996, pp. 624-625.

53. S. H. Chen and S. K. Jeng, "SBR Image Approach for Radio Wave Propagation in Tunnels with and without Traffic," *IEEE Transactions on Vehicular Technology*, **VT-45**, 3, August 1996, pp. 570-578.

54. S. H. Chen and S. K. Jeng, "An SBR/Image Approach for Radio Wave Propagation in Indoor Environments with Metallic Furniture," *IEEE Transactions on Antennas and Propagation*, **AP-45**, 1, January 1997, pp. 98-106.

55. F. Villanese, W. G. Scanlon, N. E. Evans, and E. Gambi, "Hybrid Image/Ray-Shooting UHF Radio Propagation Predictor for Populated Indoor Environments," *Electronics Letters* **35**, 21, October 1999, pp. 1804-1805.

56. M. C. Lawton and J. P. McGeehan, "The Application of a Deterministic Ray Launching Algorithm for the Prediction of Radio Channel Characteristics in Small-Cell Environments," *IEEE Transactions on Vehicular Technology*, **VT-43**, 4, November 1994, pp. 955-969.

57. U. Dersch and E. Zollinger, "Propagation Mechanisms in Microcell and Indoor Environments," *IEEE Transactions on Vehicular Technology*, **VT-43**, 4, November 1994, pp. 1058-1066.

58. K. Rizk, J. F. Wagen, and F. Gardiol, "Two-Dimensional Ray-tracing Modeling for Propagation Prediction in Microcellular Environments," *IEEE Transactions on Vehicular Technology*, **VT-46**, 2, May 1997, pp. 508-518.

59. G. M. Whitman, K. S. Kim, and E. A. Niver, "Theoretical Model for Radio Signal Attenuation Inside Buildings," *IEEE Transactions on Vehicular Technology*, **VT-44**, 3, August 1995, pp. 621-629.

60. J. H. Tarng and T. R. Liu, "Effective Models in Evaluating Radio Coverage on Single Floors of Multifloor Buildings," *IEEE Transactions on Vehicular Technology*, **VT-48**, 3, May 1999, pp. 782-789.

61. S. C. Jan and S. K. Jeng, "A Novel Propagation Modeling for Microcellular Communications in Urban Environments," *IEEE Transactions on Vehicular Technology*, **VT-46**, 4, November 1997, pp. 1021-1026.

62. W. Zhang, "Fast Two-Dimensional Diffraction Modeling for Site-Specific Propagation Prediction in Urban Microcellular Environments," *IEEE Transactions on Vehicular Technology*, **VT-49**, 2, March 2000, pp. 428-436.

63. H. Mokhtari and P. Lazaridis, "Comparative Study of Lateral Profile Knife-Edge Diffraction and Ray Tracing Technique Using GTD in Urban Environment," *IEEE Transactions on Vehicular Technology*, **VT-48**, 1, January 1999, pp. 255-261.

64. S. C. Kim, B. J. Guarino Jr., T. M. Willis III, V. Erceg, S. J. Fortune and R. A. Valenzuela, L. W. Thomas, J. Ling, and J. D. Moore, "Radio Propagation Measurements and Prediction Using Three-Dimensional Ray Tracing in Urban Environments at 908 MHz and 1.9 GHz," *IEEE Transactions on Vehicular Technology*, **VT-48**, 3, 1999, pp. 931-944.

65. J. H. Tarng, W. R. Chang, and B. J. Hsu, "Three-Dimensional Modeling of 900-MHz and 2.44-GHz Radio Propagation in Corridors," *IEEE Transactions on Vehicular Technology*, **VT-46**, 2, May 1997, pp. 519-527.

66. G. Liang and H. L. Bertoni, "A New Approach to 3-D Ray Tracing for Propagation Prediction in Cities," *IEEE Transactions on Antennas and Propagation*, **AP-46**, 6, June 1998, pp. 853-863.

67. G. Durgin, N. Patwari, and T. S. Rappaport, "Improved 3D Ray Launching Method for Wireless Propagation Prediction," *Electronics Letters*, **33**, 16, July 1997, pp. 1412-1413.

68. G. E. Athanasiadou, A. R. Nix, and J. P. McGeehan, "A Microcellular Ray-tracing Propagation Model and Evaluation of Its Narrow-Band and Wide-Band Predictions," *IEEE Journal on Selected Areas in Communications*, **18**, 3, March 2000, pp. 322-335.

69. J. P. Rossi, J. C. Bic, A. J. Levy, Y. Gabillet, and M. Rosen, "A Ray Launching Method for Radio-mobile Propagation in Urban Area," IEEE International Symposium on Antennas and Propagation *Digest*, London, Ontario, Canada, 3, 1991, pp. 1540-1543.

70. W. M. O'Brien, E. M. Kenny, and P. J. Cullen, "An Efficient Implementation of a Three-Dimensional Microcell Propagation Tool for Indoor and Outdoor Urban Environments," *IEEE Transactions on Vehicular Technology*, **VT-49**, 2, March 2000, pp. 622-630.

71. M. F. Catedra, J. Perez-Saez, F. de Adana, and O. Gutierrez, "Efficient Ray-Tracing Techniques for Three-Dimensional Analyses of Propagation in Mobile Communications: Application to Picocell and Microcell Scenarios," *IEEE Antennas and Propagation Magazine*, **40**, 2, April 1998, pp. 15-28.

72. V. Erceg, S. J. Fortune, J. Ling, A. J. Rustako Jr., and R. A. Valenzuela, "Comparisons of a Computer-Based Propagation Prediction Tool with Experimental Data Collected in Urban Microcellular Environments," *IEEE Journal on Selected Areas in Communications*, **15**, 4, May 1997, pp. 677-684.

73. J. W. Schuster and R. J. Luebbers, "Comparison of GTD and FDTD Predictions for UHF Radio Wave Propagation in a Simple Outdoor Urban Environment," IEEE International Symposium on Antennas and Propagation *Digest*, 3, 1997, pp. 2022-2025.

74. G. D. Kondylis, F. DeFlaviis, G. J. Pottie, and Y. Rahmat-Samii, "Indoor Channel Characterization for Wireless Communi-

cations Using Reduced Finite Difference Time Domain," *IEEE Vehicular Technology Conference*, **VT-3**, 1999, pp. 1402-1406.

75. A. Lauer, I. Woff, A. Bahr, J. Pamp, J. Kunisch, "Multi-Mode FDTD Simulations of Indoor Propagation Including Antenna Properties," in *Proceedings of the 1995 IEEE 45th Vehicular Technology Conference*, Chicago, IL, pp. 454-458.

76. W. Ying, S. Safavi-Naeini, and S. K. Chaudhuri, "A Hybrid Technique Based on Combining Ray Tracing and FDTD Methods for Site-Specific Modeling of Indoor Radio Wave Propagation," *IEEE Transactions on Antennas and Propagation*, **VT-48**, 5, May 2000, pp. 743-754.

77. C. Yang, B. Wu, and C. Ko, "A Ray-Tracing Method for Modeling Indoor Wave Propagation and Penetration," *IEEE Transactions on Antennas and Propagation*, **VT-46**, 6, June 1998, pp. 907-919.

78. B. De Backer, H. Borjeson, F. Olyslager, and D. De Zutter, "The Study of Wave-Propagation through a Windowed Wall at 1.8 GHz," IEEE 46th Vehicular Technology Conference, 1, 1996, pp. 165-169.

79. C. Yang and B. Wu, "Simulations and Measurements for Indoor Wave Propagation Through Periodic Structures," IEEE International Symposium on Antennas and Propagation *Digest*, **1**, 1999, pp. 384-387.

80. Z. Sandor, L. Nagy, Z. Szabo, and T. Csaba, "3D Ray Launching and Moment Method for Indoor Propagation Purposes," *The 8th IEEE International Symposium on Personal, Indoor and Mobile Radio Communications*, 1997, PIMRC '97, **1**, pp. 130-134.

81. A. Neskovic and D. Paumovic, "Indoor Electric Field Level Prediction Model Based on the Artificial Neural Networks," *IEEE Communications Letters*, **4**, 6, 2000, pp. 190-192.

82. K. E. Stocker, B. E. Gschwendtner, and F. M. Landstorfer, "Neural Network Approach to Prediction of Terrestrial Wave Propagation for Mobile Radio," *IEE Proceedings H Microwaves, Antennas and Propagation*, **140**, 4, August 1993, pp. 315-320.

83. P. Chang and W. Yang, "Environment-Adaptation Mobile Radio Propagation Prediction Using Radial Basis Function Neural Networks," *IEEE Transactions on Vehicular Technology*, **VT-46**, 1, February 1997, pp. 155-160.

84. A. A. Zaporozhets, "Application of Vector Parabolic Equation Method to Urban Radiowave Propagation Problems," *IEE Proceedings - Microwaves, Antennas and Propagation*, **146**, 4, August 1999, pp. 253-256.

85. C. Brennan and P. J. Cullen, "Application of the Fast Far-field Approximation to the Computation of UHF Path Loss Over Irregular Terrain," *IEEE Transactions on Antennas and Propagation*, **AP-46**, 6, June 1998, pp. 881-890.

86. R. Mazar and A. Bronshtein, "Propagation Model of a City Street for Personal and Microcellular Communications," *Electronics Letters*, **33**, 1, January 1997, pp. 91-92.

87. N. Blaunstein, "Average Field Attenuation in the Street Waveguide," *IEEE Transactions on Antennas and Propagation*, **AP-46**, 12, December 1998, pp. 1782-1789.

88. B. Chopard, P. O. Luthi, and J. F. Wagen, "Lattice Boltzmann Method for Wave Propagation in Urban Microcells," *IEE Proceedings - Antennas and Propagation*, **144**, 4, August 1997, pp. 251-255.

89. L. J. Greenstein, D. G. Michelson, and V. Erceg, "Moment-Method Estimation of the Ricean K-factor," *IEEE Communications Letters*, **3**, 6, June 1999, pp. 175-176.

90. V. Fung, T. S. Rappaport, and B. Thomas, "Bit Error Simulation for pi /4 DQPSK Mobile Radio Communications Using Two-ray and Measurement-based Impulse Response Models," *IEEE Journal on Selected Areas in Communications*, **11**, 3, April 1993, pp. 393-405.

91. C. C. Hess, *Handbook of Land-Mobile Radio System Coverage*, Norwood, MA, Artech House, Inc.

92. A. Safak, "Statistical Analysis of the Power Sum of Multiple Correlated Lognormal Components," *IEEE Transactions on Vehicular Technology*, **VT-42**, 1, February 1993, pp. 58-61.

93. H. Suzuki, "A Statistical Model for Urban Radio Propagation," *IEEE Transactions on Communications*, **COM-25**, 1977, pp. 673-680.

94. A. Krantzik and D. Wolf, "Analysis of a Modified Suzuki Fading Channel Model," 1989 International Conference on Acoustics, Speech, and Signal Processing, 1989 ICASSP-89, **4**, pp. 2250-2253.

95. M. Patzold, U. Killat, and F. Laue, "A Deterministic Digital Simulation Model for Suzuki Processes with Application to a Shadowed Rayleigh Land Mobile Radio Channel," *IEEE Transactions on Vehicular Technology*, **VT-45**, 2, May 1996, pp. 318-331.

96. IEEE Vehicular Technology Society Committee on Radio Propagation, "Coverage Prediction for Mobile Radio Systems Operating in the 800/900 MHz Frequency Range," *IEEE Transactions on Vehicular Technology*, **VT-37**, 1, February 1988, pp. 3-72.

97. K. Yip and T. Ng, "A Simulation Model for Nakagami-m Fading Channels, m > 1", *IEEE Transactions on Communications*, **COM-48**, 2, February 2000, pp. 214-221.

98. F. Vatalaro, "Generalized Rice-Lognormal Channel Model for Wireless Communications," *Electronics Letters*, **31**, 22, October 1995, pp. 1899-1900.

99. Y. Karasawa and H. Iwai, "Modeling of Signal Envelope Correlation of Line-of-sight Fading with Applications to Frequency Correlation Analysis," *IEEE Transactions on Communications*, **COM-42**, 6, June 1994, pp. 2201-2203.

100. T. T. Tjhung and C. C. Chai, "Fade Statistics in Nakagami-Lognormal Channels," *IEEE Transactions on Communications*, **COM-47**, 12, December 1999, pp. 1769-1772.

101. A. Abdi and M. Kaveh, "K Distribution: An Appropriate Substitute for Rayleigh-lognormal Distribution in Fading-Shadowing Wireless Channels," *Electronics Letters*, **34**, 9, April 1998, pp. 851-852.

102. G. E. Corazza and F. Vatalaro, "A Statistical Model for Land Mobile, Satellite Channels and its Application to Nongeostationary

Orbit Systems," *IEEE Transactions on Vehicular Technology*, **VT-43**, August 1994, pp. 738-741.

103. P. G. Babalis and C. N. Capsalis, "Impact of the Combined Slow and Fast Fading Channel Characteristics on the Symbol Error Probability for Multipath Dispersionless Channel Characterized by a Small Number of Dominant Paths," *IEEE Transactions on Communications*, **COM-47**, 5, May 1999, pp. 653-657.

104. D. S. Polydorou and C. N. Capsalis, "A New Theoretical Model for the Prediction of Rapid Fading Variations in Indoor Environment," *IEEE Transactions on Vehicular Technology*, **VT-46**, August 1997, pp. 748-755.

105. R. J. C. Bultitude, P. Melancon, H. Zaghloul, G. Morrison, and M. Prokki, "The Dependence of Indoor Radio Channel Multipath Characteristics of Transmit/Receiver Ranges," *IEEE Journal on Selected Areas in Communications*, **11**, 7, September 1993, pp. 979-990.

106. D. M. J. Devasirvatham, R. R. Murray, and C. Banerjee, "Time Delay Spread Measurements at 850 MHz and 1.7 GHz Inside a Metropolitan Office Building," *Electronics Letters*, **25**, 3, February 1989, pp. 194-196.

107. H. Zaghbul, M. Fattouche, G. Morrison, and D. Tholl, "Comparison of Indoor Propagation Channel Characteristics at Different Frequencies," *Electronics Letters*, **27**, 22, October 1991, pp. 2077-2079.

108. G. J. M. Janssen, P. A. Stigter, and R. Prasad, "Wideband Indoor Channel Measurements and BER Analysis of Frequency Selective Multipath Channels at 2.4, 4.75, and 11.5 GHz," *IEEE Transactions on Communications*, **COM-44**, 10, October 1996, pp. 1272-1288.

109. K. Pahlavan, R. Ganesh, and T. Hotaling, "Multipath Propagation Measurements on Manufacturing Floors at 910 MHz," *Electronics Letters*, **25**, 3, February 1989, pp. 225-227.

110. D. A. Hawbaker and T. S. Rappaport, "Indoor Wideband Radiowave Propagation Measurements at 1.3 GHz and 4.0 GHz," *Electronics Letters*, **26**, 21, October 1990, pp. 1800-1802.

111. L. Talbi and G. Y. Delisle, "Experimental Characterization of EHF Multipath Indoor Radio Channels," *IEEE Journal on Selected Areas in Communications*, **14**, 3, April 1996, pp. 431-440.

112. R. J. C. Bultitude and G. K. Bedal, "Propagation Characteristics on Microcellular Urban Mobile Radio Channels at 910 MHz," *IEEE Journal on Selected Areas in Communications*, **7**, 1, January 1989, pp. 31-39.

113. R. J. C. Bultitude, R. F. Hahn, and R. J. Davies, "Propagation Considerations for the Design of an Indoor Broad-Band Communications System at EHF," *IEEE Transactions on Vehicular Technology*, **VT-47**, 1, February 1998, pp. 235-245.

114. S. Ichitsubo, T. Furuno, T. Taga, and R. Kawasaki, "Multipath Propagation Model for Line-of-sight Street Microcells in Urban Area," *IEEE Transactions on Vehicular Technology*, **VT-49**, March 2000, pp. 422-427.

115. S. C. Kim, H. L. Bertoni, and M. Stern, "Pulse Propagation Characteristics at 2.4 GHz Inside Buildings," *IEEE Transactions on Vehicular Technology*, **VT-45**, 3, August 1996, pp. 579-592.

116. T. R. Liu and J. H. Tarng, "Modeling and Measurement of 2.44 GHz Radio Out-Of-Sight Propagation on Single Floors", *Microwave and Optical Technology Letters*, **14**, 1, January 1997, pp. 56-59.

117. R. Ganesh and K. Pahlavan, "Statistics of Short Time and Spatial Variations Measured in Wideband Indoor Radio Channels", *IEE Proceedings-H Antennas and Propagation*, **140**, 4, August 1993, pp. 297-302.

118. M. C. Lawton and J. P. McGeehan, "The Application of a Deterministic Ray Launching Algorithm for the Prediction of Radio Channel Characteristics in Small-Cell Environments," *IEEE Transactions on Vehicular Technology*, **VT-43**, 4, November 1994, pp. 955-969.

119. H. Hashemi, "Impulse Response Modeling of Indoor Radio Propagation Channels," *IEEE Journal on Selected Areas in Communications*, **11**, 7, September 1993, pp. 967-978.

120. S. Y. Seidel, T. S. Rappaport, S. Jain, M. L. Lord, and R. Singh, "Path Loss, Scattering and Multipath Delay Statistics in Four European Cities for Digital Cellular and Microcellular Radiotelephone," *IEEE Transactions on Vehicular Technology*, **VT-40**, 4, November 1991, pp. 721-730.

121. T. S. Rappaport and S. Y. Seidel, "900 MHz Multipath Propagation Measurements in Four States Cities," *Electronics Letters*, **25**, 15, July 1989, pp. 956-958.

122. T. Taga, T. Furuno, and K. Suwa, "Channel Modeling for 2-GHz-band Urban Line-of-sight Street Microcells," *IEEE Transactions on Vehicular Technology*, **VT-48**, 1, January 1999, pp. 262-272.

123. H. Son and N. Myung, "A Deterministic Ray Tube Method for Microcellular Wave Propagation Prediction Model," *IEEE Transactions on Antennas and Propagation*, **AP-47**, 8, August 1999, pp. 1344-1350.

124. L. J. Greenstein, V. Erceg, Y. S. Yeh, and M. V. Clark, "A New Path-Gain/Delay-Spread Propagation Model for Digital Cellular Channels," *IEEE Transactions on Vehicular Technology*, **VT-46**, 2, May 1997, pp. 477-485.

125. R. Ganesh and K. Pahlavan, "Statistical Modelling and Computer Simulation of Indoor Radio Channel," *IEE Proceedings I Communications, Speech and Vision*, **138**, 3, June 1991, pp. 153-161.

126. R. A. Valenzula, O. Landron, and D. L. Jacobs, "Estimating Local Mean Signal Strength of Indoor Multipath Propagation," *IEEE Transactions on Vehicular Technology*, **VT-46**, 1, February 1997, pp. 203-212.

127. G. E. Athanasiadou, A. R. Nix, and J. P. McGeehan, "A Microcellular Ray-tracing Propagation Model and Evaluation of its Narrow-Band and Wide-Band predictions," *IEEE Journal on Selected Areas in Communications*, **18**, 3, March 2000 pp. 322-335.

128. Z. Ji, B. H. Li, H. X. Wang, H. Y. Chen, and Y. G. Zhou, "An Improved Ray-Tracing Propagation Model for Predicting Path Loss on Single Floors," *Microwave and Optical Technology Letters*, **22**, 1, 1999, pp. 39-41.

129. W. K. Tam and V. N. Tran, "Multi-Ray Propagation Model for Indoor Wireless Communications," *Electronics Letters*, 32, 2, 1996, pp. 135-137.

130. K. R. Chang and H. T. Kim, "Improvement of the Computation Efficiency for a Ray-Launching model," *IEE Proceedings – Microwaves, Antennas, and Propagation*, 145, 4, 1997, pp. 303-308.

131. T. B. Gibson and D. C. Jenn, "Prediction and Measurement of Wall Insertion Loss," *IEEE Transactions on Antenna and Propagation*, AP-47, 1, 1999, pp. 55-57.

132. M. F. Iskander and Z. Yun, "Propagation Prediction Models for Wireless Communication Systems," *IEEE Transactions on Microwave Theory and Techniques*, MTT-50, 3, 2002, pp. 662-673.

133. G. Ghobadi, P. R. Shepherd, and S. R. Pennock, "2D Ray-Tracing Model for Indoor Radio Propagation at Millimeter Frequencies, and the Study of Diversity Techniques", *IEE Proceedings – Microwaves, Antennas, and Propagation*, 145, 4, 1998, pp. 349-353.

134. W. Honcharenko and H. L. Bertoni, "Transmission and Reflection Characteristics at Concrete Block Walls in the UHF Bands Proposal for Future PCs," *IEEE Transactions on Antennas and Propagation*, AP-42, 2, February 1994, pp. 232-239.

135. C. L. Holloway and P. L. Perini, "Analysis of Composite Walls and Their Effects on Short-Path Propagation Modeling," *IEEE Transactions on Vehicular Technology*, VT-46, 3, August 1997, pp. 730-738.

136. Z. Ji, B. H. Li, H. X. Wang, H. Y. Chen, and T. K. Sarkar, "Efficient Ray-Tracing Methods for Propagation Prediction for Indoor Wireless Communications," *IEEE Antennas and Propagation Magazine*, 43, 2, April 2001, pp. 41-49.

137. Z. Ji, T. K. Sarkar, and B. H. Li, "Analysis of the Effects of Walls on Indoor Wave Propagation Using the FDTD Method," *Microwave and Optical Technology Letters*, 29, 1, 2001, pp. 19-21.

138. C. A. Zelley and C. C. Constantinou, "A Three-Dimensional Parabolic Equation Applied to VHF/UHF Propagation over Irregular Terrain," *IEEE Transactions on Antennas and Propagation*, AP-47, 10, 1999, pp. 1586-1596.

139. D. J. Donohue and J. R. Kuttler, "Propagation Modeling over Terrain Using the Parabolic Wave Equation," *IEEE Transactions on Antennas and Propagation*, AP-48, 2, 2000, pp. 260-277.

140. Y. P. Zhang, Y. Hwang, and J. D. Parsons, "UHF Radio Propagation Characteristics in Straight Open-groove Structures," *IEEE Transactions on Vehicular Technology*, VT-48, 1, 1999, pp. 249-254.

141. D. Har, H. H. Xia, and H. L. Bertoni, "Path-Loss Prediction Model for Microcells," *IEEE Transactions on Vehicular Technology*, VT-48, 5, 1999, pp. 1453-1462.

142. H. L. Bertoni, W. Honcharenko, L. R. Macel, and H. H. Xia, "UHF Propagation Prediction for Wireless Personal Communications," *Proceedings of the IEEE*, 82, 9, 1994, pp. 1333-1359.

143. D. Ullmo and H. U. Baranger, "Wireless Propagation in Buildings: A Statistical Scattering Approach," *IEEE Transactions on Vehicular Technology*, VT-48, 3, 1999, pp. 947-955.

144. S. Kozono and A. Taguchi, "Mobile Propagation Loss and Delay Spread Characteristics with a Low Base Station Antenna on an Urban Road," *IEEE Transactions on Vehicular Technology*, VT-42, 1, 1993, pp. 103-109.

145. S. Obayashi and J. Zander, "A Body-Shadowing Model for Indoor Radio Communication Environments," *IEEE Transactions on Antennas and Propagation*, AP-46, 6, 1998, pp. 920-927.

146. F. Babich and G. Lombardi, "Statistical Analysis and Characterization of the Indoor Propagation Channel," *IEEE Transactions on Communications*, COM-48, 3, 2000, pp. 455-464.

147. H. Hashemi and D. Tholl, "Statistical Modeling and Simulation of the RMS Delay Spread of Indoor Radio Propagation Channels," *IEEE Transactions on Vehicular Technology*, VT-43, 1, 1993, pp. 110-120.

148. J. A. Wepman, J. R. Hoffman, and L. H. Loew, "Analysis of Impulse Response Measurements for PCS Channel Modeling Applications," *IEEE Transactions on Vehicular Technology*, VT-44, 3, 1995, pp. 613-620.

149. C. L. Holloway, M. G. Cotton, and P. McKenna, "A Model for Predicting the Power Delay Profile Characteristics Inside a Room," *IEEE Transactions on Vehicular Technology*, VT-48, 4, 1999, pp. 1110-1120.

150. P.E. Driessen, "Prediction of Multipath Delay Profiles in Mountainous Terrain," *IEEE Journal on Selected Areas in Communications*, 18, 3, 2000, pp. 336-346.

151. Y. Li, "A Theoretical Formulation for the Distribution Density of Multipath Delay Spread in a Land Mobile Radio Environment," *IEEE Transactions on Vehicular Technology*, VT-43, 2, 1994, pp. 379-388.

152. M. C. Vanderveen, C. B. Papadias, and A. Paulraj, "Joint Angle and Delay Estimation (JADE) for Multipath Signals Arriving at an Antenna Array," *IEEE Communications Letters*, 1, 1, January 1997, pp. 12 -14.

153. M. Wax and A. Leshem, "Joint Estimation of Time Delays and Directions of Arrival of Multiple Reflections of a Known Signal," *IEEE Transactions on Signal Processing*, SP-45, 10, October 1997, pp. 2477-2484.

154. M. C. Vanderveen, C. B. Papadias, and A. Paulraj, "Joint Angle and Delay Estimation (JADE) for Multipath Signals Arriving at an Antenna Array," *IEEE Communications Letters*, 1, 1, January 1997, pp. 12 -14.

155. A. J. van der Veen, M. C. Vanderveen, and A. J. Paulraj, "Joint Angle and Delay Estimation Using Shift-invariance Properties," *IEEE Signal Processing Letters*, 4, 5, May 1997, pp. 142-145.

156. A. J. van der Veen, M. C. Vanderveen, and A. J. Paulraj, "Joint Angle and Delay Estimation Using Shift-Invariance Techniques," *IEEE Transactions on Signal Processing*, SP-46, 2, February 1998, pp. 405-418.

157. M. C. Vanderveen, A. J. Van der Veen, and A. Paulraj, "Estimation of Multipath Parameters in Wireless Communications," *IEEE Transactions on Signal Processing*, **SP-46**, 3, March 1998, pp. 682-690.

158. M. C. Vanderveen, B. C. Ng, C. B. Papadias, and A. Paulraj, "Joint Angle and Delay Estimation (JADE) for Signals in Multipath Environments," *Conference Record of the Thirtieth Asilomar Conference on Signals, Systems and Computers*, **2**, 1996, pp. 250-1254.

159. B. Kannan and W. J. Fitzgerald, "Joint Angle and Delay Estimation (JADE) for Fading Multipath Signals in $\alpha$-stable noise," *in Proceedings of Signal Processing Advances in Wireless Communications*, 1999, pp. 333-336.

160. T. K. Sarkar et. al., *Smart Antennas*, New York, John Wiley and Sons, March 2003.

161. B. M. Kolundzija, J. S. Ognjanovic, and T. K. Sarkar, *WIPL-D: Electromagnetic Modeling of Composite Metallic and Dielectric Structures*, Norwood, MA, Artech House, 2000.

# Introducing the Feature Article Authors



**Tapan Kumar Sarkar** received the BTech degree from the Indian Institute of Technology, Kharagpur, India, in 1969; the MScE degree from the University of New Brunswick, Fredericton, Canada, in 1971; and the MS and PhD degrees from Syracuse University, Syracuse, New York in 1975.

From 1975 to 1976, he was with the TACO Division of General Instruments Corporation. He was with the Rochester Institute of Technology, Rochester, NY, from 1976 to 1985. He was a Research Fellow at the Gordon McKay Laboratory, Harvard University, Cambridge, MA, from 1977 to 1978. He is now a Professor in the Department of Electrical and Computer Engineering, Syracuse University, Syracuse, NY. His current research interests deal with numerical solutions of operator equations arising in electromagnetics and signal processing with application to system design. He obtained one of the "best solution" awards in May, 1977, at the Rome Air Development Center (RADC) Spectral Estimation Workshop. He has authored or coauthored ten books, including most recently *Iterative and Self Adaptive Finite-Elements in Electromagnetic Modeling* and *Wavelet Applications in Engineering Electromagnetics*, which were published in 1998 and 2002, respectively by Artech House. He has published more than 210 journal articles and numerous conference papers, and has written chapters in 28 books. His book on *Smart Antennas* will be published by John Wiley in March, 2003.

Dr. Sarkar is a registered Professional Engineer in the State of New York. He received the Best Paper Award of the *IEEE*

*Transactions on Electromagnetic Compatibility* in 1979, and for the 1997 National Radar Conference. He received the College of Engineering Research Award in 1996, and the Chancellor's Citation for Excellence in Research in 1998 at Syracuse University. He was elected Fellow of the IEEE in 1991. He was an Associate Editor for Feature Articles of the *IEEE Antennas and Propagation Society Newsletter*, and he was the Technical Program Chairman for the 1988 IEEE International Symposium on Antennas and Propagation and USNC/URSI National Radio Science Meeting. Currently, he is a Distinguished Lecturer for the IEEE Antennas and Propagation Society. He is on the editorial boards of *Journal of Electromagnetic Waves and Applications* and *Microwave and Optical Technology Letters*. He has been a US National Committee representative to many URSI General Assemblies. He was the Chair of the URSI Inter-Commission Working Group on Time-Domain Metrology (1990-1996). Dr. Sarkar is a member of Sigma Xi and USNC/URSI Commissions A and B. He received the title Docteur Honoris Causa from Universite Blaise Pascal, Clermont Ferrand, France, in 1998, and the Friends of Clermont Ferrand award in 2000.



**Zhong Ji** received both the BS and MS degrees in Electronic Engineering from Shandong University, China, in 1988 and 1991, respectively. He received the PhD degree from Shanghai Jiao Tong University, China, in 2000.

He was a teacher of Shandong University from 1991 to 1997. He is currently a Research Associate with Syracuse University, Syracuse, NY. His research interests are in the areas of propagation models for wireless communications, and time-domain analysis of electromagnetic fields.

**Kyungjung Kim** was born in Seoul, Korea. He received the BS degree from Inha University, Korea, and the MS degree from Syracuse University, Syracuse, NY. He is currently working towards the PhD degree in the Department of Electrical Engineering at Syracuse University.

He was a Research Assistant at Syracuse University from 1998 to 2001, and has been a Graduate Fellow since 2001. His current research interests include digital signal processing related to adaptive antenna problems and wavelet transforms.

**Abdellatif Medouri** was born in Tetouan, Morocco, on December 11, 1965. He received the BS degree in Physics from University Abdelmalek Essaadi, Tetouan, Morocco, in 1989, and the PhD degree from the University of Granada, Spain, in 1995. He was a research student from 1989 to 1995 in the Department of Applied Physics, University of Granada, Spain. He was a Research Scientist at the National Research Center of Morocco from 1996 to 2001. He is currently a professor at the National School of Applied Physics, Tangier, Morocco. His research interests include sensor

array signal processing, identification of radar targets, and high-order statistics.



**Magdalena Salazar-Palma** was born in Granada, Spain. She received the PhD degree in Ingeniero de Telecomunicación from the Universidad Politécnica de Madrid (Spain), where she is a Professor Titular of the Departamento de Señales, Sistemas y Radiocomunicaciones (Signals, Systems and Radiocommunications Department) at the Escuela Técnica Superior de Ingenieros de Telecomunicación of the same university. She has taught courses on electromagnetic field theory, microwave and antenna theory, circuit networks and filter theory, analog and digital communication systems theory, and numerical methods for electromagnetic field problems, as well as related laboratories. Her research within the Grupo de Microoondas y Radar (Microwave and Radar Group) is in the areas of electromagnetic field theory, and computational and numerical methods for microwave structures, passive components, and antenna analysis; design, simulation, optimization, implementation, and measurements of hybrid and monolithic microwave integrated circuits; and network and filter theory and design.

She has authored a total of 10 contributions for chapters and articles in books, 15 papers in international journals, and 75 papers in international symposiums and workshops, plus a number of national publications and reports. She has lectured in several short courses, some of them in the framework of European Community Programs. She has participated in 19 projects and contracts, financed by international, European, and national institutions and companies. She has been a member of the Technical Program Committee of several international symposiums, and has acted as reviewer for international scientific journals. She has assisted the Comisión Interministerial de Ciencia y Tecnología (National Board of Research) in the evaluation of projects. She has also served in several evaluation panels of the Commission of the European Communities. She has acted in the past as topical Editor for the disk of references of the *Review of Radio Science*. She is a member of the editorial board of two scientific journals. She has served as Vice Chair and Chair of the IEEE MTT/AP-S Spanish Joint Chapter, and is currently serving as Chair of the Spain Section of the IEEE. She has received two individual research awards from national institutions. ⊛

implementation and further discussion with IEEE IT staff, Dan Senese told me that the use of this spam-labeling software would be offered to IEEE alias-account users only on an "opt-in" basis. I think that's an excellent solution. I salute and thank Dan Senese and the IEEE staff for their willingness to listen, and for making the decision they did.

You'll have to decide for yourself whether or not you want the IEEE to implement such filtering on your e-mail, if you use an IEEE e-mail alias. For now, at least, I plan not to. Because my opposition to this is not just a matter of practicality, but also of principle, I hope I never have to. If I were ever to do so, I would never turn the final decision about the disposition of an e-mail message so labeled over to software: the potential consequence of a "false positive" is too great. At least, now *you'll* be able to make the decision for yourself.

A final note: As this is going to press, I have yet another situation in which my e-mails to an author are being rejected as spam, even though I've tried sending them via two e-mail accounts with totally different ISPs. This is beginning to be as serious a problem as the spam, itself!

## Thank You!

At the Columbus Symposium, I was very honored and grateful to receive the AP-S Outstanding Service Award for being Editor of the *Newsletter* and Editor-in-Chief of the *Magazine*. Actually, the wording of the citation was very nice and somewhat more detailed; you can read it, along with information about the other AP-S and IEEE awards presented there to AP-S members, in Allan Schell's report of the Awards and Fellow Committee in this issue. I'm going to take the liberty of repeating most of the comments I made in receiving the award, because it's important that all of those who have been such an important part of creating and sustaining these publications be recognized.

One of the most rewarding aspects of editing the *Magazine* is that I get to work with a large number of very wonderful people. This includes the many AP-S members who contribute what we publish. Without them, we have no *Magazine*. Thank you! It also includes our Staff, a dedicated group of professionals who have given selflessly of their time and talents. Without them there also would be no *Magazine*, and they must share this award: I accepted it, in part, on their behalf. Thanks, too, to all of you, our readers. Your support is what has made the *Magazine* possible. Finally, I wouldn't be able to edit the *Magazine* without the constant love, support, and giving up of time I would otherwise spend with them by my wife and daughter. My thanks to them – and to all of you, again.

One of the best things about this award is that I get to keep on editing the *Magazine*. Thank you for the award – and for the wonderful support of our AdComs and Officers and members, through the years and now, in letting me continue to do this job!

*Ross*